Fast Iterative Semi-Blind Receiver for URLLC in Short-Frame Full-Duplex Systems with CFO

Yujie Liu, *Student Member, IEEE,* Xu Zhu, *Senior Member, IEEE,* Eng Gee Lim, *Senior Member, IEEE,* Yufei Jiang, *Member, IEEE,* and Yi Huang, *Senior Member, IEEE*

***Abstract*—We propose an iterative semi-blind (ISB) receiver structure to enable ultra-reliable low-latency communications (URLLC) in short-frame full-duplex (FD) systems with carrier frequency offset (CFO). To the best of our knowledge, this is the first work to propose an integral solution to channel estimation and CFO estimation for short-frame FD systems by utilizing a single pilot. By deriving an equivalent system model with CFO included implicitly, a subspace based blind channel estimation is proposed for the initial stage, followed by CFO estimation and channel ambiguities elimination. Then refinement of channel and CFO estimates is conducted iteratively. The integer and fractional parts of CFO in the full range are estimated as a whole and in closed-form at each iteration. The proposed ISB receiver significantly outperforms the previous methods in terms of frame error rate (FER), mean square errors (MSEs) of channel estimation and CFO estimation and output signal-to-interference-and-noise ratio (SINR), while at a halved spectral overhead. Cramér-Rao lower bounds (CRLBs) are derived to verify the effectiveness of the proposed ISB receiver structure. It also demonstrates high computational efficiency as well as fast convergence speed.**

***Index Terms*—Ultra-reliable low-latency communications (URLLC), full duplex (FD), short frame, self-interference cancelation (SIC), carrier frequency offset (CFO).**

I. Introduction

The fifth generation (5G) wireless communications are expected to support three types of services: enhanced mobile broadband (eMBB), massive machine-type communications (mMTC) and ultra-reliable low-latency communications (URLLC) [1]–[5]. URLLC, supporting the transmission of information with stringent requirements on reliability and latency, is a key technology for numerous emerging applications, such as tactile Internet, factory automation, virtual reality, intelligent transport systems, etc [1]–[5]. However, URLLC design has a great challenge: how to reduce the end-to-end latency while achieving similar reliability, which has attracted much attention from researchers.

There are several surveys in the literature, which provided helpful insights of URLLC design. It is claimed in [1] that reliability can be enhanced through frequency and space diversity, robust channel coding schemes (Turbo codes, low density parity check codes (LDPC), polar codes) [6], multi-connectivity, retransmission, etc. A comprehensive survey of latency reduction solutions was provided in [2] from three aspects: 1) radio access network (RAN), 2) core network and 3) caching. From the perspective of RAN, latency can be minimized by shortening the transmission time interval (TTI) duration (short-frame transmission) [7]–[9], advanced multiple access techniques (*e.g.*, generalized frequency division multiplexing (GFDM) [10] , filter bank multi-carrier (FBMC) [11], universal filtered multi-carrier (UFMC) [11], non-orthogonal multiple access (NOMA) [12], [13]), grant-free radio access [14], full duplex (FD) [15], [16], etc. Most existing work on URLLC focused on shortening the frame length, through reducing either the symbol duration (increasing the subcarrier spacing) or the number of symbols per TTI [1].

A. Related Work

Short-frame communications have two serious problems as follows. On one hand, classical information-theoretic performance metrics relevant for long frames, *i.e.*, ergodic capacity and outage capacity, are no longer applicable for short frames, since the law of large number cannot be applied [7]. To tackle this, new performance metrics were introduced for short frames in [7], namely maximum coding rate at finite frame length and finite frame error probability. Based on these, the performance of NOMA in short-frame communications was investigated in both [12] and [13] and it was concluded that NOMA has a much superior performance than orthogonal multiple access (OMA) in terms of both latency and throughput. Also, a wireless-powered communication network at finite frame length regime was studied in [9] and [17], respectively.

On the other hand, the length of pilot is a challenging issue in short-frame communications [7], [8], [18], [19]. Pilot transmission is important for a reliable receiver design, such

Manuscript received June 22, 2018; revised December 10, 2018; accepted January 25, 2019. This work was supported in part by the Department for Digital, Culture, Media and Sport, U.K., through the Liverpool 5G Project, in part by the Science and Technology Innovation Commission of Shenzhen under Grant JCYJ20170307151258279, and in part by the Natural Science Foundation of Guangdong Province under Grant 2018A030313344. (*Corresponding author: Xu Zhu.*)

Y. Liu is with the Department of Electrical Engineering and Electronics, University of Liverpool, Liverpool L69 3GJ, U.K., and also with the Department of Electrical and Electronic Engineering, Xi'an Jiaotong-Liverpool University, Suzhou 215123, China (e-mail:yujieliu@liverpool.ac.uk).

X. Zhu is with the Department of Electrical Engineering and Electronics, University of Liverpool, Liverpool L69 3GJ, U.K. (e-mail: xuzhu@liverpool.ac.uk).

E. G. Lim is with the Department of Electrical and Electronic Engineering, Xi'an Jiaotong-Liverpool University, Suzhou 215123, China (e-mail:enggee.lim@xjtlu.edu.cn).

Y. Jiang is with the School of Electronic and Information Engineering, Harbin Institute of Technology, Shenzhen 518055, China (e-mail:jiangyufei@hit.edu.cn).

Y. Huang is with the Department of Electrical Engineering and Electronics, University of Liverpool, Liverpool L69 3GJ, U.K. (e-mail: yi.huang@liverpool.ac.uk).

as obtaining a good synchronization and channel estimation, which requires a large number of pilots. However, a large number of pilots are likely to reduce the useful data rate fraction in short-frame communications, resulting in low spectral efficiency. The impact of pilot length on the performance of short-frame physical-layer network coding systems was studied and random coding bound was utilized to identify good pilot-length regimes [18]. The authors in [19] optimized the pilot overhead for short-frame communications and studied the relationship between the pilot overhead and the frame length and error probability. To overcome the reduced training overhead due to short frames, the detected data symbols were utilized to further enhance the reliability of short-frame communications in [8].

FD communication, which allows simultaneous transmission and reception at the same frequency, can double the transmission rate and reduce the end-to-end latency [2], [3], [20], [21]. However, much less work on short-frame communications has considered it. When introducing FD to short-frame communications, two research problems can be investigated: 1) how much throughput can FD achieve at finite frame length regime, in comparison to half-duplex (HD) mode? and 2) with limited pilot and data symbols, how to design a high-reliability receiver for FD systems? Regarding the first problem, Gu *et al.* analyzed and compared the performance of FD and HD relaying for URLLC and concluded that FD relaying is more preferable [15]. However, its superior performance is achieved only if self-interference (SI) resulting from FD transmission has been canceled to a reasonable level. Hence, the second question to design a reliable receiver is very essential. To the best of the authors' knowledge, it is still an open area in the literature.

One of the major challenges of FD implementation is the SI from its transmitter to its own receiver. In FD orthogonal frequency division multiplexing (OFDM) systems, there are mainly three techniques to cancel SI for detection of the desired signal, namely passive cancelation (PC) [22], [23], analog cancelation (AC) [22], [24] and digital cancelation (DC) [22], [25]–[32]. PC is the first stage of SI cancelation, which is achieved by antenna placement, directional antenna, antenna shielding, etc. [22], [23]. In the second stage, SI is further mitigated in the analog domain before the low-noise amplifier and analog-to-digital converter to avoid overloading/saturation [22], [24]. DC is the last stage of SI cancelation, which estimates the SI channel, creates a replica of the received SI and then cancels it from the received signal in the digital domain. In this paper, we focus on SI cancelation in the digital domain.

Several DC methods have been proposed in the literature for long-frame communications. A least-square (LS) based SI channel estimator was proposed in [22], however, which treats the desired signal as additive noise, degrading the system performance. A two-stage LS cancelation scheme was presented in [28], which iterates between SI cancelation and signal detection. However, its performance requires a good initial estimate of the desired channel. An iterative maximum-likelihood (ML) channel estimator was described for the estimation of both SI and desired channels in [29], by utilizing the known SI, the pilots and unknown data symbols of the desired signal. Nevertheless, it has high training overhead, due to the consecutive pilot transmission for a long period. When applied to short-frame communications, it has a significant performance degradation. Koohian proposed a superimposed signaling technique to cancel SI and detect the desired signal without requiring the procedure of channel estimation [25]. However, its SI channel is assumed to be flat fading only, and thus it cannot be utilized if frequency selective channel fading exists. In [32], a subspace based algorithm was proposed to jointly estimate the coefficients of both SI and desired channels and transceiver impairments. However, it requires lots of data symbols to achieve a good second-order statistics of received signal, which performs poorly if applied to short-frame communications.

Meanwhile, when considering system impairments, the existing work on FD systems with long frames usually considered IQ imbalances at transmitter and/or receiver [30]–[32], phase noises [29], [31] and power amplifier nonlinearities [31], [32], and only a few considered carrier frequency offset (CFO). CFO is usually incurred by the mismatch between local oscillators at the transmitter and receiver or a Doppler frequency shift. When CFO is present, the reliability of FD systems degrades greatly. CFO estimation and compensation are well-researched problems in HD OFDM systems [33]–[35]. However, it is not straightforward to apply them to FD OFDM systems, since the compensation of CFO based on the desired signal would introduce a CFO to the SI. Only a few works in the literature have investigated CFO in FD systems. A frequency synchronization technique was developed in [26] for FD systems. Nevertheless, it requires long training sequences and its pilots of the desired signal and SI should be non-overlapping, *i.e.*, sent in different time slots, resulting in high training overhead and latency. Meanwhile, its integer and fractional parts of CFO are estimated separately, requiring two processes and suffering error propagations. A two-step synchronization structure was proposed in [27] that synchronizes based on SI firstly and then the desired signal. However, the first synchronization step treats the desired signal as noise, resulting in poor performance, and it considers fractional CFO only. Furthermore, both [26] and [27] did not consider the estimation of desired channel.

B. Contributions

In this paper, an iterative semi-blind (ISB) receiver structure with CFO and channel estimation and signal detection is proposed for URLLC in short-frame FD cyclic-prefix (CP) OFDM systems. By deriving an equivalent system model with CFO included implicitly, a subspace based blind channel estimation is proposed for the initial stage, followed by CFO estimation and channel ambiguities elimination assisted by a single pilot. Then refinement of channel and CFO estimates is conducted iteratively. Our work is different in the following aspects.

- To the best of the authors' knowledge, this is the first work to propose a high-reliability receiver structure for

short-frame FD CP-OFDM systems in the presence of CFO. The proposed ISB receiver structure requires only a short frame to calculate the second-order statistics of the received signal, which is about tens of times less than the existing semi-blind methods [29], [32]. It significantly outperforms the methods in [29], [32], [34] and [35] in terms of frame error rate (FER), mean square errors (MSEs) of channel estimation and CFO estimation and output signal-to-interference-and-noise ratio (SINR). Cramér-Rao lower bounds (CRLBs) on the MSEs of channel estimation, CFO estimation and signal detection are derived for the first time for short-frame FD CP-OFDM systems, which verify the effectiveness of the proposed ISB receiver structure.

- This is the first work to provide an integral solution to channel estimation and CFO estimation for FD CP-OFDM systems by utilizing a single pilot, considering their impact on each other, while in [22], [25]–[31] and [32] only one of the issues was addressed assuming perfect estimation of the other and also two training processes were required to estimate CFO and channels separately. The joint semi-blind CFO and channel estimation for zero-padding (ZP) based multiuser OFDM systems in [33] is not applicable for widely-applied CP-OFDM systems. Also, the hard decisions of signals are exploited to refine both CFO and channel estimates iteratively, while in [8] and [29] only channel estimation was iterated assuming perfect CFO estimation and compensation.
- The proposed ISB receiver enables high spectral efficiency with only a single pilot required for joint CFO estimation and channel ambiguities elimination. Its training overhead is much lower than that of [29], [32], [34] and [35]. A single pilot for both the desired signal and SI is carefully designed and superimposed to enable simultaneous transmission of them in FD training mode, while the pilots of multiple users for joint CFO and channel estimation in ZP-OFDM systems [33] are sent in different time slots, resulting in reduced spectral efficiency. It also converges fast within 3 iterations, and is more computationally efficient than the iterative ML approach [29].
- The integer and fractional parts of CFO in the full range are estimated as a whole with a closed-form solution rather than separately as in [26], [27], [34] and [35], without suffering error propagation. The closed-form solution is independent of iCFO estimation range and does not require an advanced acquisition of iCFO range, unlike the iCFO estimator in [34]. CFO compensation is performed on the desired signal estimates, avoiding the introduction of CFO to the SI by the methods in [26] and [27].

C. Organization and Notations

The rest of this paper is organized as follows. Section II describes the short-frame FD CP-OFDM system and derives an equivalent system with CFO included implicitly. The proposed ISB receiver structure is given in Sections III and IV. Section III illustrates the initial stage of the proposed ISB receiver structure while Section IV demonstrates the iterative decision-directed stages. Performance analysis and simulation results are given in Sections V and VI. Section VII draws conclusion.

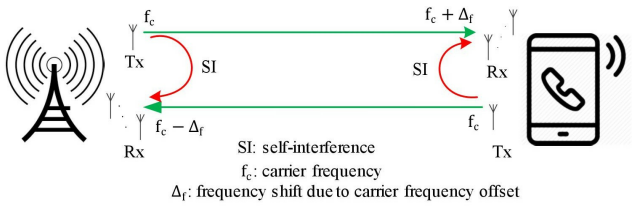

Fig. 1. A bidirectional FD CP-OFDM system in the presence of CFO.

Bold symbols represent vectors/matrices, and superscripts T, $*$, H and $\dagger$ denote the transpose, complex conjugate, complex conjugate transpose and pseudo inverse of a vector/matrix, respectively. diag$\{\mathbf{a}\}$ is a diagonal matrix with vector $\mathbf{a}$ on its diagonal. $\mathbf{I}_N$ is a N-dimensional identity matrix. $\mathbf{0}_{M\times N}$ is a $M \times N$ zero matrix. $\mathbf{1}_{M\times N}$ is an all-one $M \times N$ matrix. $\mathbb{E}\{\}$ is the expectation operator. $\otimes$ is the Kronecker product. $\Re\{\mathbf{A}\}$ and $\Im\{\mathbf{A}\}$ are the real and imaginary parts of a complex matrix $\mathbf{A}$. $\jmath$ is the basic imaginary unit. $[\mathbf{A};\mathbf{B}]$ and $[\mathbf{A},\mathbf{B}]$ denote that $\mathbf{A}$ and $\mathbf{B}$ are concatenated by rows and columns, respectively. circshift$(\cdot)$ and toeplitz$(\cdot)$ are Matlab functions to shift array circularly and to create a Toeplitz matrix, respectively. $\bar{\mathbf{A}}$ indicates a transformation of $\mathbf{A}$ by incorporating CFO. $\mathbf{A}_\mathrm{s}$ and $\mathbf{A}_\mathrm{i}$ denote the matrix for desired signal and SI, respectively. $\mathbf{A}'_j$ represents the estimate of $\mathbf{A}$ in the j-th iteration of the proposed ISB receiver structure.

II. System Model

A. Short-Frame FD CP-OFDM System

We consider a bidirectional short-frame FD CP-OFDM system in the presence of CFO, where the base station (BS) and mobile station (MS) operate in FD scheme, as illustrated in Fig. 1. The BS and MS are equipped with a single transmit antenna and N_r receive antennas. Due to the inherent symmetry, MS is chosen as our research object, as the same performance can be observed at BS. The signal transmitted from BS to MS is referred to as the desired signal while the signal transmitted from MS to MS is SI. In the following, we focus on digital cancelation of the residual SI after passive and analog cancelation.

Each short frame consists of T OFDM symbols with N subcarriers each. The transmit vectors corresponding to the t-th $(t = 0, \cdots, T-1)$ OFDM symbol for the desired signal and SI are given by $\mathbf{x}_{\mathrm{s},t} = [x_{\mathrm{s},t}(0), x_{\mathrm{s},t}(1), \cdots, x_{\mathrm{s},t}(N-1)]^T$ and $\mathbf{x}_{\mathrm{i},t} = [x_{\mathrm{i},t}(0), x_{\mathrm{i},t}(1), \cdots, x_{\mathrm{i},t}(N-1)]^T$, respectively, where $x_{\mathrm{s},t}(n)$ and $x_{\mathrm{i},t}(n)$ are the corresponding symbols on subcarrier n $(n = 0, 1, \cdots, N-1)$. Each OFDM symbol $\mathbf{x}_{\mathrm{s},t}$ and $\mathbf{x}_{\mathrm{i},t}$ are processed by Inverse Discrete Fourier Transform (IDFT), and then a cyclic prefix (CP) of length L_cp is pre-pended. The transmit signal vectors of the desired signal and SI in the time domain are denoted as $\mathbf{s}_{\mathrm{s},t} = [s_{\mathrm{s},t}(0), s_{\mathrm{s},t}(1), \cdots, s_{\mathrm{s},t}(M-1)]^T$ and $\mathbf{s}_{\mathrm{i},t} = [s_{\mathrm{i},t}(0), s_{\mathrm{i},t}(1), \cdots, s_{\mathrm{i},t}(M-1)]^T$, respectively, with $M = N + L_\mathrm{cp}$.

Define $\mathbf{h}_{\rm s}^{n_{\rm r}} = [h_{\rm s}^{n_{\rm r}}(0), h_{\rm s}^{n_{\rm r}}(1), \cdots, h_{\rm s}^{n_{\rm r}}(L-1)]^T$ and $\mathbf{h}_{\rm i}^{n_{\rm r}} = [h_{\rm i}^{n_{\rm r}}(0), h_{\rm i}^{n_{\rm r}}(1), \cdots, h_{\rm i}^{n_{\rm r}}(L-1)]^T$ as the respective desired and SI channel impulse response (CIR) vectors for the $n_{\rm r}$-th receive antenna, with L being the length of CIR. The channels are assumed to exhibit quasi-static block fading and the CIRs remain constant for a short frame's duration. Define $\phi = \phi_{\rm i} + \phi_{\rm f}$ ($\phi \in (-N/2, N/2]$) as the CFO between the BS and MS, where $\phi_{\rm i}$ and $\phi_{\rm f}$ are the respective integer CFO (iCFO) and fractional CFO (fCFO). The SI does not experience CFO assuming all the transmit and receive antennas of MS share one local oscillator [26], [27]. The received signal in the t-th symbol at the $n_{\rm r}$-th ($n_{\rm r} = 0, 1, \cdots, N_{\rm r}-1$) receive antenna in the time domain can be written as

$$y_t^{n_{\rm r}}(m) = e^{j2\pi\phi m/N} \sum\nolimits_{l=0}^{L-1} h_{\rm s}^{n_{\rm r}}(l) s_{{\rm s},t}(m-l) + \sqrt{\frac{1}{\rho}} \sum\nolimits_{l=0}^{L-1} h_{\rm i}^{n_{\rm r}}(l) s_{{\rm i},t}(m-l) + w_t^{n_{\rm r}}(m) \quad (1)$$

where ρ is the average input desired signal-to-SI-ratio, denoted as SIR, before digital cancelation, and $w_t^{n_{\rm r}}(m)$ ($m = 0, 1, \cdots, M-1$) is the noise term.

B. Equivalent System with CFO Included Implicitly

According to (1), it can be observed that the received signal is corrupted by both CFO and SI, making the desired signal detection more challenging. The existing methods require two separate training processes for the respective CFO and channel estimation, suffering from high training overhead and high latency [22], [25]–[32]. In the following, an equivalent system model with CFO included implicitly is derived so that CFO and channel can be estimated jointly with a single pilot. By incorporating the CFO into the desired signal and channel, (1) is equivalent to

$$y_t^{n_{\rm r}}(m) = \sum\nolimits_{l=0}^{L-1} \bar{h}_{\rm s}^{n_{\rm r}}(l) \bar{s}_{{\rm s},t}(m-l) + \sqrt{\frac{1}{\rho}} \sum\nolimits_{l=0}^{L-1} h_{\rm i}^{n_{\rm r}}(l) s_{{\rm i},t}(m-l) + w_t^{n_{\rm r}}(m) \quad (2)$$

where $\bar{h}_{\rm s}^{n_{\rm r}}(l) = e^{j2\pi\phi l/N} h_{\rm s}^{n_{\rm r}}(l)$ and $\bar{s}_{{\rm s},t}(m) = e^{j2\pi\phi m/N} s_{{\rm s},t}(m)$ are denoted as the respective CFO-included channel and CFO-included desired signal in the equivalent system model. It is worth noticing that SI and its channel are not modified since it does not experience CFO.

Among the received signal samples in CP, $y_t^{n_{\rm r}}(L-1)$ to $y_t^{n_{\rm r}}(L_{\rm cp}-1)$ are free from inter-symbol interference, and hence are utilized alongside signal samples $y_t^{n_{\rm r}}(L_{\rm cp})$ to $y_t^{n_{\rm r}}(M-1)$ for estimation of CFO and channels. Collecting all these samples from $N_{\rm r}$ received antennas into a vector yields $\mathbf{y}_t = [y_t^0(L-1), y_t^1(L-1), \cdots, y_t^{N_{\rm r}-1}(L-1), \cdots, y_t^0(M-1), y_t^1(M-1), \cdots, y_t^{N_{\rm r}-1}(M-1)]^T$, which is formulated as

$$\mathbf{y}_t = \bar{\mathbf{H}} \bar{\mathbf{s}}_t + \mathbf{w}_t \quad (3)$$

where $\bar{\mathbf{H}} = [\bar{\mathbf{H}}_{\rm s}, \mathbf{H}_{\rm i}]$, with $\bar{\mathbf{H}}_{\rm s}$ of size $(M-L+1)N_{\rm r} \times M$ defined as

$$\bar{\mathbf{H}}_{\rm s} = \begin{bmatrix} \bar{\mathbf{h}}_{\rm s}(L-1) & \cdots & \bar{\mathbf{h}}_{\rm s}(0) & \cdots & \cdots & \mathbf{0}_{N_{\rm r}\times 1} \\ \vdots & \ddots & \ddots & \ddots & \ddots & \vdots \\ \mathbf{0}_{N_{\rm r}\times 1} & \cdots & \cdots & \bar{\mathbf{h}}_{\rm s}(L-1) & \cdots & \bar{\mathbf{h}}_{\rm s}(0) \end{bmatrix} \quad (4)$$

$\bar{\mathbf{h}}_{\rm s}(l) = [\bar{h}_{\rm s}^0(l), \bar{h}_{\rm s}^1(l), \cdots, \bar{h}_{\rm s}^{N_{\rm r}-1}(l)]^T$, $\mathbf{H}_{\rm i}$ is defined as the same form to $\bar{\mathbf{H}}_{\rm s}$ but with $\bar{\mathbf{h}}_{\rm s}(l)$ replaced by $\mathbf{h}_{\rm i}(l) = \sqrt{\frac{1}{\rho}}[h_{\rm i}^0(l), h_{\rm i}^1(l), \cdots, h_{\rm i}^{N_{\rm r}-1}(l)]^T$; $\bar{\mathbf{s}}_t = [\bar{\mathbf{s}}_{{\rm s},t}^T, \mathbf{s}_{{\rm i},t}^T]^T$, with $\bar{\mathbf{s}}_{{\rm s},t} = [\bar{s}_{{\rm s},t}(0), \bar{s}_{{\rm s},t}(1), \cdots, \bar{s}_{{\rm s},t}(M-1)]^T$ and $\mathbf{s}_{{\rm i},t} = [s_{{\rm i},t}(0), s_{{\rm i},t}(1), \cdots, s_{{\rm i},t}(M-1)]^T$; $\mathbf{w}_t = [w_t^0(L-1), w_t^1(L-1), \cdots, w_t^{N_{\rm r}-1}(L-1), \cdots, w_t^0(M-1), w_t^1(M-1), \cdots, w_t^{N_{\rm r}-1}(M-1)]^T$. It is easily found that the rank of $\mathbb{E}\{\bar{\mathbf{s}}_t \bar{\mathbf{s}}_t^H\}$ is $2N$ instead of $2M$ due to the redundancy from CP. Since $\mathbb{E}\{\bar{\mathbf{s}}_t \bar{\mathbf{s}}_t^H\}$ is rank deficient, (3) cannot be applied to the subspace based blind channel estimation methods [36], [37].

To address this problem, we form $(L_{\rm cp}+1)$ subvectors of size $(N-L+1)N_{\rm r} \times 1$ from $\mathbf{y}_t$, and the g-th ($g = 0, 1, \cdots, L_{\rm cp}$) subvector is denoted as

$$\begin{aligned} \mathbf{y}_{t,g} = & [y_t^0(L-1+g), y_t^1(L-1+g), \cdots, \\ & y_t^{N_{\rm r}-1}(L-1+g), \cdots, y_t^0(N-1+g), \\ & y_t^1(N-1+g), \cdots, y_t^{N_{\rm r}-1}(N-1+g)]^T \end{aligned} \quad (5)$$

which is written as

$$\mathbf{y}_{t,g} = \tilde{\mathbf{H}} \bar{\mathbf{s}}_{t,g} + \mathbf{w}_{t,g}, \quad g = 0, 1, \cdots, L_{\rm cp} \quad (6)$$

where $\tilde{\mathbf{H}} = [\tilde{\mathbf{H}}_{\rm s}, \tilde{\mathbf{H}}_{\rm i}]$, with $\tilde{\mathbf{H}}_{\rm s}$ and $\tilde{\mathbf{H}}_{\rm i}$ following the similar form to $\bar{\mathbf{H}}_{\rm s}$ but with a reduced size of $(N-L+1)N_{\rm r} \times N$ instead of $(M-L+1)N_{\rm r} \times M$; $\bar{\mathbf{s}}_{t,g} = [\bar{\mathbf{s}}_{{\rm s},t,g}^T, \mathbf{s}_{{\rm i},t,g}^T]^T$ with $\bar{\mathbf{s}}_{{\rm s},t,g} = [\bar{s}_{{\rm s},t}(g), \bar{s}_{{\rm s},t}(g+1), \cdots, \bar{s}_{{\rm s},t}(N-1+g)]^T$ and $\mathbf{s}_{{\rm i},t,g} = [s_{{\rm i},t}(g), s_{{\rm i},t}(g+1), \cdots, s_{{\rm i},t}(N-1+g)]^T$; $\mathbf{w}_{t,g} = [w_t^0(L-1+g), w_t^1(L-1+g), \cdots, w_t^{N_{\rm r}-1}(L-1+g), \cdots, w_t^0(N-1+g), w_t^1(N-1+g), \cdots, w_t^{N_{\rm r}-1}(N-1+g)]^T$.

Since $\mathbb{E}\{\bar{\mathbf{s}}_{t,g} \bar{\mathbf{s}}_{t,g}^H\}$ is full rank with $2N$, (6) can be applied to the subspace based blind channel estimation methods, as long as $\tilde{\mathbf{H}}$ is a tall matrix which can be achieved by setting $(N-L+1)N_{\rm r} > 2N$. Meanwhile, thanks to the partition of the received signal into several subvectors, the second-order statistics of the received signal can be achieved by utilizing a short frame with a small number of OFDM symbols. It is noteworthy that such an equivalent system model was derived for ZP-OFDM systems in [33], however which cannot be applied here for widely-used CP-OFDM systems and also requires a large number of symbols to achieve the second-order statistics of the received signal.

Based on the equivalent system model derived, an ISB receiver structure is proposed for URLLC in short-frame FD CP-OFDM systems in the presence of CFO, which consists of two kinds of stages. On one hand, the CFO and channel estimation as well as signal detection are performed initially by the proposed subspace based semi-blind method, referred to as the initial stage. On the other hand, the initial estimation and detection performance are enhanced significantly by performing iterations among them, where the previous hard decisions are utilized to overcome the pilot shortage due to

the short frame structure, referred to as iterative decision-directed stages. The block diagram of the proposed ISB receiver structure is illustrated in Fig. 2.

III. Initial Stage of the ISB Receiver Structure

First, a subspace based blind method is proposed to estimate the CFO-included desired channel and SI channel with some ambiguities, which requires a very short frame to obtain the second-order statistics of the received signal. Second, a single pilot for the desired signal and SI is carefully designed and superimposed to enable simultaneous transmission of them to achieve FD training mode, and the corresponding channel ambiguities and CFO can be extracted jointly by the parametric channel estimation method. Third, based on the CFO-included desired and SI channel estimates, the received SI is generated and canceled from the received signal, and then the desired signal can be easily detected.

A. Blind Channel Estimation

A subspace based blind channel estimator is proposed to jointly estimate the CFO-included desired channel and SI channel, by utilizing a short frame. We assume that 1) noise samples are uncorrelated and 2) noise and signal samples are uncorrelated. By utilizing $N_{\rm r}$ receive antennas with $(N-L+1)N_{\rm r} > 2N$, the proposed estimator is summarized in four steps below.

Step 1. $(T-1)$ received data symbols within a short frame are used to compute the auto-correlation matrix of the received signal, obtaining

$$\mathbf{R}_{\rm y} = \frac{1}{(T-1)(L_{\rm cp}+1)} \sum_{t=1}^{T-1} \sum_{g=0}^{L_{\rm cp}} \mathbf{y}_{t,g} \mathbf{y}_{t,g}^H \tag{7}$$

It is worth noting that the number of signal samples per received symbol used to compute the auto-correlation matrix of the received signal has been increased, thanks to the partition of the received signal vector $\mathbf{y}_t$ into a number of subvectors $\mathbf{y}_{t,g}$ when deriving the equivalent system model. Thus, the required frame length T to achieve the second-order statistics of the received signal can be much shorter than the methods in [32], [33], [36] and [37].

Step 2. Eigenvalue decomposition (EVD) is performed on the auto-correlation matrix $\mathbf{R}_y$. The signal subspace has a dimension of $2N$, while the noise subspace has Q $(Q = (N-L+1)N_{\rm r} - 2N)$ eigenvectors corresponding to the smallest Q eigenvalues of the matrix $\mathbf{R}_y$. Denote the q-th eigenvector as $\boldsymbol{\gamma}_q = [\boldsymbol{\gamma}_q^T(0), \boldsymbol{\gamma}_q^T(1), \cdots, \boldsymbol{\gamma}_q^T(N-L)]^T$ $(q = 0, 1, \cdots, Q-1)$, where $\boldsymbol{\gamma}_q(m)$ is a column vector of size $N_{\rm r}$. Due to the inherent orthogonality between the signal and noise subspaces, the columns of $\tilde{\mathbf{H}}$ are orthogonal to each vector $\boldsymbol{\gamma}_q$ $(q = 0, 1, \cdots, Q-1)$, *i.e.*,

$$\boldsymbol{\gamma}_q^H \tilde{\mathbf{H}} = \mathbf{0}_{1\times 2N} \tag{8}$$

Therefore, $\boldsymbol{\gamma}_q$ spans the left null space of $\tilde{\mathbf{H}}$. Since $\tilde{\mathbf{H}}$ is formulated by the matrices $\bar{\mathbf{h}}_{\rm s}(l)$ and $\mathbf{h}_{\rm i}(l)$, $(l = 0, 1, \cdots, L-1)$, we can restrict channel estimation to $\bar{\mathbf{h}}_{\rm s}(l)$ and $\mathbf{h}_{\rm i}(l)$, instead of the whole matrix $\tilde{\mathbf{H}}$.

Step 3. Defining $\bar{\mathbf{h}}(l) = [\bar{\mathbf{h}}_{\rm s}(l), \mathbf{h}_{\rm i}(l)]$, it can be found (8) is equivalent to the following equations:

$$\begin{aligned}
&\textstyle\sum_{l=L-1-n}^{L-1} \boldsymbol{\gamma}_q^H(l-L+1+n)\bar{\mathbf{h}}(l) = \mathbf{0}_{1\times 2},\\
&\text{for } n = 0, 1, \cdots, L-2\\
&\textstyle\sum_{l=0}^{L-1} \boldsymbol{\gamma}_q^H(n-L+1+l)\bar{\mathbf{h}}(l) = \mathbf{0}_{1\times 2},\\
&\text{for } n = L-1, L, \cdots, N-L\\
&\textstyle\sum_{l=0}^{N-1-n} \boldsymbol{\gamma}_q^H(n-L+1+l)\bar{\mathbf{h}}(l) = \mathbf{0}_{1\times 2},\\
&\text{for } n = N-L+1, \cdots, N-1
\end{aligned} \tag{9}$$

or in the following matrix form:

$$\boldsymbol{\Theta}_q \bar{\mathbf{h}} = \mathbf{0}_{N\times 2} \tag{10}$$

and $\boldsymbol{\Theta}_q$ of size $N \times N_{\rm r}L$ is given by

$$\boldsymbol{\Theta}_q = \begin{bmatrix}
\boldsymbol{\gamma}_q^H(a) & \mathbf{0}_{1\times N_{\rm r}} & \cdots & \mathbf{0}_{1\times N_{\rm r}} \\
\boldsymbol{\gamma}_q^H(a-1) & \boldsymbol{\gamma}_q^H(a) & \cdots & \mathbf{0}_{1\times N_{\rm r}} \\
\vdots & \vdots & \ddots & \vdots \\
\boldsymbol{\gamma}_q^H(b+1) & \boldsymbol{\gamma}_q^H(b+2) & \cdots & \boldsymbol{\gamma}_q^H(a) \\
\boldsymbol{\gamma}_q^H(b) & \boldsymbol{\gamma}_q^H(b+1) & \cdots & \boldsymbol{\gamma}_q^H(a-1) \\
\vdots & \vdots & \ddots & \vdots \\
\boldsymbol{\gamma}_q^H(0) & \boldsymbol{\gamma}_q^H(1) & \cdots & \boldsymbol{\gamma}_q^H(L-1) \\
\mathbf{0}_{1\times N_{\rm r}} & \boldsymbol{\gamma}_q^H(0) & \cdots & \boldsymbol{\gamma}_q^H(L-2) \\
\vdots & \vdots & \ddots & \vdots \\
\mathbf{0}_{1\times N_{\rm r}} & \mathbf{0}_{1\times N_{\rm r}} & \cdots & \boldsymbol{\gamma}_q^H(0)
\end{bmatrix} \tag{11}$$

where $a = N-L$, $b = N-2L$, and $\bar{\mathbf{h}} = [\bar{\mathbf{h}}^T(0), \bar{\mathbf{h}}^T(1), \cdots, \bar{\mathbf{h}}^T(L-1)]^T$ is with size $N_{\rm r}L \times 2$.

Step 4. Considering all $\boldsymbol{\Theta}_q$ $(q = 0, 1, \cdots, Q-1)$ matrices as follows

$$\boldsymbol{\Theta} = [\boldsymbol{\Theta}_0^T, \boldsymbol{\Theta}_1^T, \cdots, \boldsymbol{\Theta}_{Q-1}^T]^T \tag{12}$$

We can obtain

$$\boldsymbol{\Theta}\bar{\mathbf{h}} = \mathbf{0}_{NQ\times 2} \tag{13}$$

Hence, $\bar{\mathbf{h}}$ can be estimated by choosing the 2 right singular vectors of $\boldsymbol{\Theta}$, denoted as $\bar{\mathbf{h}}_0$. However, there exist ambiguities between the real CFO-included channel $\bar{\mathbf{h}}$ and the blindly estimated CFO-included channel $\bar{\mathbf{h}}_0$, *i.e.*,

$$\bar{\mathbf{h}} = \bar{\mathbf{h}}_0 \mathbf{b} \tag{14}$$

where $\mathbf{b}$ with a dimension of 2×2 is the complex channel ambiguity matrix. The first and second columns of $\bar{\mathbf{h}}_0$ are the respective CFO-included desired channel and SI channel by the subspace based blind channel estimation approach, denoted as $\bar{\mathbf{h}}_{\rm s,0}$ and $\mathbf{h}_{\rm i,0}$, respectively. The proposed subspace based blind channel estimation algorithm is depicted in Algorithm 1. In the following, a single pilot is carefully designed to enable the joint CFO estimation and channel ambiguities elimination.

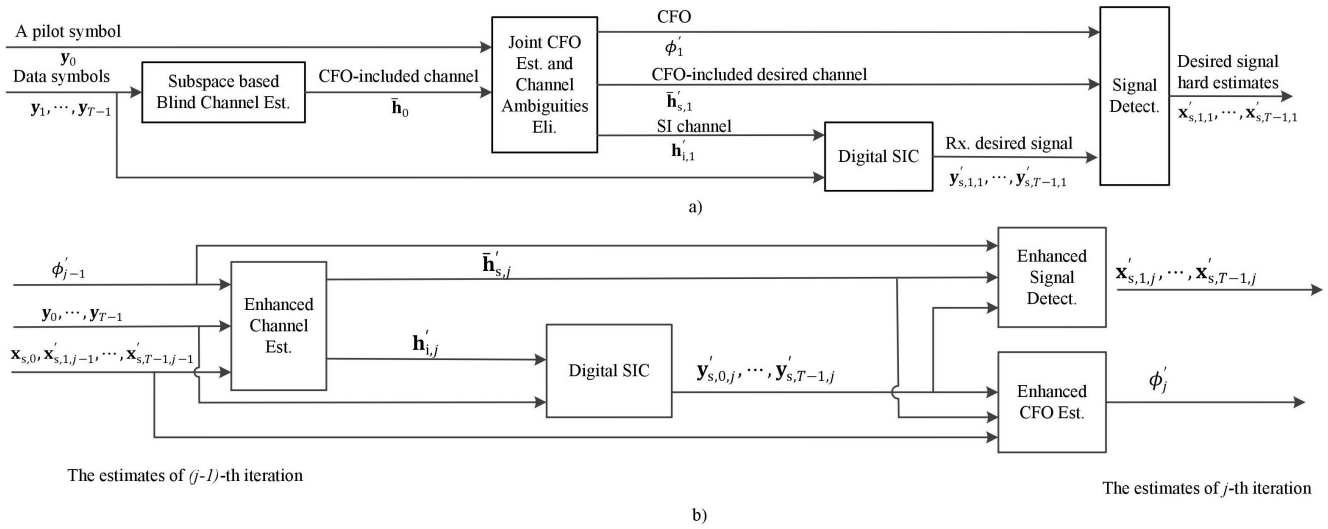

Fig. 2. a) initial stage and b) the j-th ($j \geq 2$) iterative decision-directed stage of the proposed ISB receiver structure (Est.: estimation, SIC: SI cancelation and Detect.: detection).

Algorithm 1 Subspace based blind channel estimation.

Input:

The received data symbol subvectors, $\mathbf{y}_{t,g}$, $t = 1, 2, \cdots, T-1$, $g = 0, 1, \cdots, L_{\mathrm{cp}}$;

Output:

CFO-included desired channel and SI channel estimates, $\bar{\mathbf{h}}_{\mathrm{s},0}$ and $\mathbf{h}_{\mathrm{i},0}$;

1: Compute the auto-correlation matrix of the received signal by (7), obtaining $\mathbf{R}_{\mathrm{y}}$;
2: Obtain Q eigenvectors, corresponding to the smallest Q eigenvalues of the matrix $\mathbf{R}_{\mathrm{y}}$;
3: Form matrix $\mathbf{\Theta}_q$ according to (11);
4: Obtain the CFO-included desired channel and SI channel estimates, by choosing the 2 right singular vectors of $\mathbf{\Theta}$;
5: **return** $\bar{\mathbf{h}}_{\mathrm{s},0}$, $\mathbf{h}_{\mathrm{i},0}$.

B. Pilot Design

A single pilot of the desired signal and SI is well designed to enable simultaneous transmission of them to achieve FD training mode so that the corresponding CFO and channel ambiguities can be extracted jointly by the parametric channel estimation methods.

With the channel estimates by the proposed subspace based blind method, (6) can be rewritten as

$$\mathbf{y}_{t,g} = \bar{\mathbf{H}}_0 \mathbf{B}_{\mathrm{s}} \bar{\mathbf{s}}_{\mathrm{s},t,g} + \bar{\mathbf{H}}_0 \mathbf{B}_{\mathrm{i}} \mathbf{s}_{\mathrm{i},t,g} + \mathbf{w}_{t,g} \tag{15}$$

where $\bar{\mathbf{H}}_0$ is defined as the same form to $\bar{\mathbf{H}}_{\mathrm{s}}$ but with $\bar{\mathbf{h}}_{\mathrm{s}}(l)$ replaced by $\bar{\mathbf{h}}_0(l)$; $\mathbf{B}_{\mathrm{s}} = \mathbf{I}_N \otimes \mathbf{b}_{\mathrm{s}}$ and $\mathbf{B}_{\mathrm{i}} = \mathbf{I}_N \otimes \mathbf{b}_{\mathrm{i}}$ with $\mathbf{b}_{\mathrm{s}}$ and $\mathbf{b}_{\mathrm{i}}$ being the first and second columns of $\mathbf{b}$, respectively. By multiplying the received signal $\mathbf{y}_{t,g}$ with the pseudoinverse of $\bar{\mathbf{H}}_0$, we can obtain

$$\mathbf{r}_{t,g} = \mathbf{B}_{\mathrm{s}} \bar{\mathbf{s}}_{\mathrm{s},t,g} + \mathbf{B}_{\mathrm{i}} \mathbf{s}_{\mathrm{i},t,g} + \tilde{\mathbf{w}}_{t,g} \tag{16}$$

where $\tilde{\mathbf{w}}_{t,g} = \bar{\mathbf{H}}_0^{\dagger} \mathbf{w}_{t,g}$. Then, $\mathbf{r}_{t,g}$ is divided into N column vectors of length 2, and $\mathbf{r}_{t,g}(n) = [\mathbf{r}_{t,g}(n), \mathbf{r}_{t,g}(n+N)]^T$, for $n = 0, 1, \cdots, N-1$, and $\mathbf{r}_{t,g}(n)$ is given by

$$\begin{aligned} \mathbf{r}_{t,g}(n) =& \mathbf{b}_{\mathrm{s}} e^{j2\pi\phi(n+g)/N} \mathbf{s}_{\mathrm{s},t,g}(n) \\ &+ \mathbf{b}_{\mathrm{i}} \mathbf{s}_{\mathrm{i},t,g}(n) + \tilde{\mathbf{w}}_{t,g}(n) \end{aligned} \tag{17}$$

where $\tilde{\mathbf{w}}_{t,g}(n)$ is a column vector of length 2 and $\tilde{\mathbf{w}}_{t,g} = [\tilde{\mathbf{w}}_{t,g}^T(0), \tilde{\mathbf{w}}_{t,g}^T(1), \cdots, \tilde{\mathbf{w}}_{t,g}^T(N-1)]^T$.

According to (17), it can be observed that as long as $\mathbf{s}_{\mathrm{s},t,g}(0) = \cdots = \mathbf{s}_{\mathrm{s},t,g}(N-1) = c$ and $\mathbf{s}_{\mathrm{i},t,g}(0) = \cdots = \mathbf{s}_{\mathrm{i},t,g}(N-1) = d$, (17) can be rewritten as

$$\mathbf{r}_{t,g}(n) = \mathbf{b} e^{j2\pi\boldsymbol{\phi}(n+g)/N} + \tilde{\mathbf{w}}_{t,g}(n) \tag{18}$$

where $\boldsymbol{\phi} = [\phi, 0]^T$. For simplicity, c and d have been specified as 1. It can be noticed that (17) looks like the channel frequency response model in [38]. Therefore, parametric channel estimation methods, *e.g.*, estimation of signal parameters via rotational invariance technique (ESPRIT) [38] and LS, can be exploited here to estimate the CFO and channel ambiguities, respectively. By utilizing all $(L_{\mathrm{cp}}+1)$ subvectors of the received pilot symbol $\mathbf{y}_t$, it is easily obtained that the transmitted pilot ought to meet $s_{\mathrm{s},t}(m) = 1$ and $s_{\mathrm{i},t}(m) = 1$ for $m = 0, 1, \cdots, M-1$. In this paper, we assume the first OFDM symbol $t = 0$ is transmitted for training.

It is noteworthy that two pilot patterns have also been designed in [33] to jointly estimate the CFOs and channel ambiguities for multiuser ZP-OFDM systems. However, to avoid multiuser interferences, the pilots of different users should be non-overlapping, resulting in reduced spectral efficiency. In contrast, our proposed pilot design can be overlapping, which is indeed designed for FD systems. Meanwhile, the CFO and channel ambiguities can be extracted jointly by utilizing a single pilot. Therefore, the FD training mode and low training overhead make it more applicable for URLLC.

C. Joint CFO Estimation and Channel Ambiguities Elimination

As discussed earlier, with the pilot design, the estimation problem of CFO and channel ambiguities relates to the parametric channel estimation problem. Thus, the time delay estimator, *e.g.*, ESPRIT, in the parametric channel estimation, can be exploited here to extract the unknown CFO, while the path amplitude estimator, *e.g.*, LS, can be used to determine the channel ambiguities.

1) CFO Estimation: Utilizing the ESPRIT algorithm, the CFO estimation is summarized in four steps below:

Step 1. Form the matrix $\mathbf{r}_{\text{pil},g} = [\mathbf{r}_{0,g}(0), \cdots, \mathbf{r}_{0,g}(N-1)]^T$ with size $N \times 2$, and it can be expressed as

$$\mathbf{r}_{\text{pil},g} = \mathbf{V}_g \mathbf{b}^T + \tilde{\mathbf{w}}_{\text{pil},g} \tag{19}$$

where $\mathbf{V}_g = [\mathbf{V}_g(\phi), \mathbf{V}(0)]$ with $\mathbf{V}_g(\phi) = [e^{j2\pi\phi g/N}, \cdots, e^{j2\pi\phi(N-1+g)/N}]^T$ and $\mathbf{V}(0) = \mathbf{1}_{N\times 1}$, and $\tilde{\mathbf{w}}_{\text{pil},g} = [\tilde{\mathbf{w}}_{0,g}(0), \cdots, \tilde{\mathbf{w}}_{0,g}(N-1)]^T$

Step 2. Compute the auto-correlation matrix of $\mathbf{r}_{\text{pil},g}$ considering all the received subvector samples of the pilot symbol,

$$\mathbf{R}_{\text{r}} = \frac{1}{2(L_{\text{cp}}+1)} \sum\nolimits_{g=0}^{L_{\text{cp}}} \mathbf{r}_{\text{pil},g} \mathbf{r}_{\text{pil},g}^H \tag{20}$$

Hence, the auto-correlation matrix has been averaged by $(L_{\text{cp}}+1)$, thanks to the partition of the received signal into a number of subvectors, which can enhance the CFO estimation. It is also worth noting the auto-correlation matrix has been averaged by 2, which results from the ambiguities incurred by the blind channel estimation. $\mathbf{R}_{\text{r}}$ is further improved by the forward-backward (FB) averaging technique [38], obtaining

$$\mathbf{R}_{\text{FB,r}} = \frac{1}{2}(\mathbf{R}_{\text{r}} + \mathbf{J}\mathbf{R}_{\text{r}}^*\mathbf{J}) \tag{21}$$

where $\mathbf{J}$ is the $N \times N$ matrix whose components are zero except for ones on the anti-diagonal.

Step 3. 2 eigenvectors corresponding to the largest 2 eigenvalues of $\mathbf{R}_{\text{FB,r}}$ are found, denoted as $\mathbf{u}$ of size $N \times 2$. Due to the phase rotational invariance property, there exists the following relationship $\mathbf{u}_2 = \mathbf{u}_1 \text{diag}\{e^{j2\pi\boldsymbol{\phi}/N}\}$ where $\mathbf{u}_1$ and $\mathbf{u}_2$ of size $(N-1)\times 2$ are the first $(N-1)$ and last $(N-1)$ rows of $\mathbf{u}$ respectively.

Step 4. The CFO can be extracted by

$$\boldsymbol{\phi}_1' = \frac{\angle \boldsymbol{\delta} N}{2\pi} \tag{22}$$

where $\boldsymbol{\delta}$ is the eigenvalues of $\mathbf{u}_1^\dagger \mathbf{u}_2$, and the subscript $_1$ denotes this is the initial estimation. It is worth noticing that $\boldsymbol{\phi}_1'$ consists of two CFOs. The one with the largest absolute value is the unknown CFO ϕ, *i.e.*, $\phi_1' = \max|\boldsymbol{\phi}_1|$, since the CFO of SI is always 0. Note that CFO has been estimated in one step where the integer and fractional parts of CFO are estimated as a whole and with a closed-form solution, unlike the existing methods in [26], [27], [34] and [35].

2) Channel Ambiguities Elimination: The channel ambiguities can then be computed by the LS method, with the CFO estimate ϕ_1'. It involves two steps.

Step 1. Form the matrix $\mathbf{V}_g' = [\mathbf{V}_g(\phi_1'), \mathbf{V}(0)]$.

Step 2. According to (19), the channel ambiguities are estimated by the LS method, *i.e.*,

$$\mathbf{b}' = ((\mathbf{V}_{\text{pil}}')^\dagger \mathbf{r}_{\text{pil}})^T \tag{23}$$

where $\mathbf{V}_{\text{pil}}' = [\mathbf{V}_0'; \mathbf{V}_1'; \cdots; \mathbf{V}_{L_{\text{cp}}}']$ and $\mathbf{r}_{\text{pil}} = [\mathbf{r}_{\text{pil},0}; \mathbf{r}_{\text{pil},1}; \cdots; \mathbf{r}_{\text{pil},L_{\text{cp}}}]$. Thus, the desired and SI channel ambiguity vectors are obtained as $\mathbf{b}_{\text{s}}'$ and $\mathbf{b}_{\text{i}}'$ by choosing the first and second columns of $\mathbf{b}'$, respectively.

Step 3. The CFO-included desired and SI channel estimates are obtained as

$$\bar{\mathbf{h}}_{\text{s},1}' = \bar{\mathbf{h}}_0 \mathbf{b}_{\text{s}}', \quad \mathbf{h}_{\text{i},1}' = \bar{\mathbf{h}}_0 \mathbf{b}_{\text{i}}' \tag{24}$$

Define $\bar{\mathbf{H}}_{\text{s},1}'$ and $\mathbf{H}_{\text{i},1}'$ as the circulant desired and SI channel matrices, following the same form to $\bar{\mathbf{H}}_{\text{s}}$ and $\mathbf{H}_{\text{i}}$ with replacing $\bar{\mathbf{h}}_{\text{s}}$ and $\mathbf{h}_{\text{i}}$ by $\bar{\mathbf{h}}_{\text{s},1}'$ and $\mathbf{h}_{\text{i},1}'$, respectively.

Algorithm 2 Joint CFO estimation and channel ambiguities elimination.

Input:
The received pilot subvectors, $\mathbf{r}_{0,g}(n)$, with $n = 0, 1, \cdots, N-1$, $g = 0, 1, \cdots, L_{\text{cp}}$;
The blind channel estimate, $\bar{\mathbf{h}}_0$;

Output:
CFO estimate, ϕ_1';
CFO-included desired and SI channel estimates, $\bar{\mathbf{h}}_{\text{s},1}'$ and $\mathbf{h}_{\text{i},1}'$;

1: Form the matrix $\mathbf{r}_{\text{pil},g}$;
2: Compute the auto-correlation matrix of $\mathbf{r}_{\text{pil},g}$, obtaining $\mathbf{R}_{\text{FB,r}}$ by (20) and (21);
3: Find 2 eigenvectors corresponding to the largest 2 eigenvalues of $\mathbf{R}_{\text{FB,r}}$, denoted as $\mathbf{u}$;
4: Estimate CFO by (22);
5: Form the matrix $\mathbf{V}_g'$;
6: Estimate channel ambiguities by (23);
7: Obtain the CFO-included desired channel and SI channel estimates through (24);
8: **return** ϕ_1', $\bar{\mathbf{h}}_{\text{s},1}'$ and $\mathbf{h}_{\text{i},1}'$.

D. SI Cancelation and Signal Detection

With the SI channel estimate, the received SI can be generated and canceled from the received signal, obtaining $\mathbf{y}_{\text{s},t,1}' = \mathbf{y}_t - \mathbf{H}_{\text{i},1}' \mathbf{s}_{\text{i},t}$. With the CFO estimate ϕ_1', the desired signal in the time domain is estimated by

$$\mathbf{s}_{\text{s},t,1}' = \mathbf{E}(\phi_1')(\bar{\mathbf{H}}_{\text{s},1}')^\dagger \mathbf{y}_{\text{s},t,1}' \tag{25}$$

where $\mathbf{E}(\phi_1') = \text{diag}\{[1, e^{-j2\pi\phi_1'/N}, \cdots, e^{-j2\pi\phi_1'(M-1)/N}]\}$. Define $\mathbf{d}_{t,1}$ of size $N \times 1$ as the desired signal estimate in the time domain. $\mathbf{d}_{t,1}(n) = \mathbf{s}_{\text{s},t,1}'(n + L_{\text{cp}})$ for $n = 0, 1, \cdots, N - L_{\text{cp}} - 1$. As the first L_{cp} elements of $\mathbf{s}_{\text{s},t,1}'$ are the CP, the last L_{cp} elements of $\mathbf{d}_{t,1}$ can be refined by

$$\begin{aligned}\mathbf{d}_{t,1}(n) =& \frac{1}{2}(\mathbf{s}_{\text{s},t,1}'(n + L_{\text{cp}}) + \mathbf{s}_{\text{s},t,1}'(n - N + L_{\text{cp}})) \\ & \text{for } n = N - L_{\text{cp}}, \cdots, N-1\end{aligned} \tag{26}$$

It is noteworthy that CFO compensation has been performed on the CFO-included desired signal estimate instead of the

received signal, avoiding the introduction of CFO to SI by the existing methods [26], [27]. By performing Discrete Fourier Transform (DFT) on $\mathbf{d}_{t,1}$, the frequency-domain desired signal is detected, and the hard estimate is obtained as $\mathbf{x}'_{\mathrm{s},t,1}$.

IV. Iterative Decision-Directed Stages of the ISB Receiver Structure

To mitigate the impact of short training overhead due to the short frame, the hard decisions are utilized to enhance channel estimation, signal detection and CFO estimation iteratively. First, the enhanced CFO-included desired channel and SI channel estimates are determined by the previous desired signal estimates, the pilot and the known SI. Then, a more accurate SI cancelation is performed. Last, the desired signal estimate is refined, while an enhanced CFO estimate is obtained thanks to the inherent relationship between the previous desired signal estimate and the newly CFO-included desired signal estimate. The iterative channel estimation, signal detection and CFO estimation algorithm is shown in Algorithm 3.

A. Enhanced Channel Estimation, SI Cancelation and Signal Detection

It is easy to show that (3) is equivalent to

$$\mathbf{y}_t = \bar{\mathbf{S}}_{\mathrm{s},t}\bar{\mathbf{h}}_{\mathrm{s}} + \mathbf{S}_{\mathrm{i},t}\mathbf{h}_{\mathrm{i}} + \mathbf{w}_t \tag{27}$$

where

$$\bar{\mathbf{S}}_{\mathrm{s},t} = \begin{bmatrix} \dot{\mathbf{s}}_{\mathrm{s},t}(L-1) & \dot{\mathbf{s}}_{\mathrm{s},t}(L-2) & \cdots & \dot{\mathbf{s}}_{\mathrm{s},t}(0) \\ \dot{\mathbf{s}}_{\mathrm{s},t}(L) & \dot{\mathbf{s}}_{\mathrm{s},t}(L-1) & \cdots & \dot{\mathbf{s}}_{\mathrm{s},t}(1) \\ \vdots & \vdots & \ddots & \vdots \\ \dot{\mathbf{s}}_{\mathrm{s},t}(M-1) & \dot{\mathbf{s}}_{\mathrm{s},t}(M-2) & \cdots & \dot{\mathbf{s}}_{\mathrm{s},t}(M-L) \end{bmatrix} \tag{28}$$

with $\dot{\mathbf{s}}_{\mathrm{s},t}(m) = \mathbf{I}_{N_{\mathrm{r}}} \otimes \bar{s}_{\mathrm{s},t}(m)$ and $\mathbf{S}_{\mathrm{i},t}$ follows the same form to $\bar{\mathbf{S}}_{\mathrm{s},t}$, but with $\bar{s}_{\mathrm{s},t}(m)$ replaced by $s_{\mathrm{i},t}(m)$.

The hard decision can be utilized to refine channel estimation iteratively. By performing IDFT on the previous desired signal hard estimate in the $(j-1)$-th iteration $\mathbf{x}'_{\mathrm{s},t,j-1}$, the time-domain desired signal with CP insertion is determined as $\tilde{\mathbf{s}}'_{\mathrm{s},t,j-1}$, and the CFO-included signal is obtained as $\bar{\mathbf{s}}'_{\mathrm{s},t,j-1} = \mathbf{E}(-\phi'_{j-1})\tilde{\mathbf{s}}'_{\mathrm{s},t,j-1}$. Note that the first symbol $(t=0)$ is pilot and is always known at the receiver, thus $\mathbf{x}'_{\mathrm{s},0,j-1} = \mathbf{x}_{\mathrm{s},0}$ regardless of the value of j. Then, $\bar{\mathbf{S}}'_{\mathrm{s},t,j-1}$ can be easily obtained by replacing $\bar{s}_{\mathrm{s},t}(m)$ in $\bar{\mathbf{S}}_{\mathrm{s},t}$ by $\bar{\mathbf{s}}'_{\mathrm{s},t,j-1}(m)$. Therefore, the CFO-included desired and SI channels can be enhanced by

$$[\bar{\mathbf{h}}'_{\mathrm{s},j}; \mathbf{h}'_{\mathrm{i},j}] = (\bar{\mathbf{S}}'_{j-1})^{\dagger}\tilde{\mathbf{y}} \tag{29}$$

where $\bar{\mathbf{S}}'_{j-1} = [\bar{\mathbf{S}}'_{\mathrm{s},0,j-1}, \mathbf{S}_{\mathrm{i},0}; \cdots; \bar{\mathbf{S}}'_{\mathrm{s},T-1,j-1}, \mathbf{S}_{\mathrm{i},T-1}]$ and $\tilde{\mathbf{y}} = [\mathbf{y}_0; \mathbf{y}_1; \cdots; \mathbf{y}_{T-1}]$.

Similarly, the size-reduced circulant desired channel matrix is obtained as $\tilde{\mathbf{H}}'_{\mathrm{s},j}$ following the form of $\tilde{\mathbf{H}}_{\mathrm{s}}$ with $\bar{\mathbf{h}}_{\mathrm{s}}$ replaced by $\bar{\mathbf{h}}'_{\mathrm{s},j}$, while the circulant desired and SI channel matrices $\bar{\mathbf{H}}'_{\mathrm{s},j}$ and $\mathbf{H}'_{\mathrm{i},j}$ are determined following the form of $\bar{\mathbf{H}}_{\mathrm{s}}$, with $\bar{\mathbf{h}}_{\mathrm{s}}$ replaced by $\bar{\mathbf{h}}'_{\mathrm{s},j}$ and $\mathbf{h}'_{\mathrm{i},j}$, respectively. Then, SI is canceled from the received signal, obtaining $\mathbf{y}'_{\mathrm{s},t,j} = \mathbf{y}_t - \mathbf{H}'_{\mathrm{i},j}\mathbf{s}_{\mathrm{i},t}$. With the new estimates $\bar{\mathbf{H}}'_{\mathrm{s},j}$ and $\mathbf{y}'_{\mathrm{s},t,j}$ and the previous CFO estimate ϕ'_{j-1}, the new hard estimate of the desired signal can be obtained as $\mathbf{x}'_{\mathrm{s},t,j}$ by utilizing (25) and (26). It is noteworthy that the CFO included in the desired channel and signal should be the same in the derived equivalent system model. As the CFO-included desired channel estimate $\bar{\mathbf{H}}'_{\mathrm{s},j}$ is obtained by the previous CFO estimate ϕ'_{j-1}, the hard estimate of the desired signal should be determined by performing CFO compensation with the previous CFO estimate.

B. Enhanced CFO Estimation

To enhance CFO estimation, we divide the estimated received signal vector $\mathbf{y}'_{\mathrm{s},t,j}$ into $(L_{\mathrm{cp}}+1)$ subvectors, and the g-th $(g = 0, 1, \cdots, L_{\mathrm{cp}})$ subvector is defined as

$$\begin{aligned} \mathbf{y}'_{\mathrm{s},t,j,g} = [&\mathbf{y}'_{\mathrm{s},t,j}(gN_{\mathrm{r}}), \mathbf{y}'_{\mathrm{s},t,j}(gN_{\mathrm{r}}+1), \cdots, \\ &\mathbf{y}'_{\mathrm{s},t,j}(gN_{\mathrm{r}}+N_{\mathrm{r}}-1), \cdots, \mathbf{y}'_{\mathrm{s},t,j}((g+N-L)N_{\mathrm{r}}), \\ &\mathbf{y}'_{\mathrm{s},t,j}((g+N-L)N_{\mathrm{r}}+1), \\ &\cdots, \mathbf{y}'_{\mathrm{s},t,j}((g+N-L)N_{\mathrm{r}}+N_{\mathrm{r}}-1)] \end{aligned} \tag{30}$$

Similarly to (6), $\mathbf{y}'_{\mathrm{s},t,j,g}$ is given by

$$\mathbf{y}'_{\mathrm{s},t,j,g} = \tilde{\mathbf{H}}_{\mathrm{s}}\bar{\mathbf{s}}_{\mathrm{s},t,g} + \mathbf{z}_{t,g} \tag{31}$$

where $\mathbf{z}_{t,g}$ is the noise term. With the new CFO-included desired channel estimate $\tilde{\mathbf{H}}'_{\mathrm{s},j}$, the CFO-included desired signal is estimated by

$$\bar{\mathbf{s}}'_{\mathrm{s},t,j,g} = (\tilde{\mathbf{H}}'_{\mathrm{s},j})^{\dagger}\mathbf{y}'_{\mathrm{s},t,j,g} \tag{32}$$

Algorithm 3 Iterative channel estimation, signal detection and CFO estimation.

Input:
- Frequency domain desired signal estimate, $\mathbf{x}'_{\mathrm{s},t,j-1}$, $t = 0, 1, \cdots, T-1$;
- Frequency domain SI signal, $\mathbf{x}_{\mathrm{i},t}$, $t = 0, 1, \cdots, T-1$;
- CFO estimate, ϕ'_{j-1};
- Time domain received signal, $\mathbf{y}_t$, $t = 0, 1, \cdots, T-1$;

Output:
- CFO-included desired channel and SI channel estimates, $\bar{\mathbf{h}}'_{\mathrm{s},j}$ and $\mathbf{h}'_{\mathrm{i},j}$;
- Frequency domain desired signal estimate, $\mathbf{x}'_{\mathrm{s},t,j}$;
- CFO estimate, ϕ'_j;

1: Refine the CFO-included desired channel and SI channel by (29);
2: Refine SI cancelation, obtaining the received desired signal $\mathbf{y}'_{\mathrm{s},t,j}$;
3: Obtain the refined desired signal estimate, $\mathbf{x}_{\mathrm{s},t,j}$, by (25) and (26);
4: Form $(L_{\mathrm{cp}}+1)$ subvectors from $\mathbf{y}'_{\mathrm{s},t,j}$ by (30);
5: Determine the CFO-included desired signal estimate by (32);
6: Compute the CFO vector by (34);
7: Calculate the auto-correlation of the CFO vector through (35);
8: Obtain the refined CFO estimate, ϕ'_j, following the similar procedures of Steps 3 and 4 of Algorithm 2;
9: **return** $\bar{\mathbf{h}}'_{\mathrm{s},j}$, $\mathbf{h}'_{\mathrm{i},j}$, $\mathbf{x}'_{\mathrm{s},t,j}$ and ϕ'_j.

There exists an inherent relationship between the reestimated CFO-included desired signal $\bar{\mathbf{s}}'_{\mathrm{s},t,j,g}$ and the previous desired signal estimate $\mathbf{s}'_{\mathrm{s},t,j-1,g}$ in the ideal case, *i.e.*,

$$\bar{\mathbf{s}}'_{\mathrm{s},t,j,g} = \mathrm{diag}\{\mathbf{V}_g(\phi)\}\mathbf{s}'_{\mathrm{s},t,j-1,g} \tag{33}$$

where $\mathbf{s}'_{\mathrm{s},t,j-1,g} = [\tilde{\mathbf{s}}'_{\mathrm{s},t,j-1}(g), \cdots, \tilde{\mathbf{s}}'_{\mathrm{s},t,j-1}(g+N-1)]^T$. Therefore, utilizing all the previous desired signal estimates $(t = 0, \cdots, T-1)$, the CFO can be further enhanced by the ESPRIT algorithm as follows.

Step 1. Compute the CFO vector $\mathbf{e}_{t,g} = [e_{t,g}(0), e_{t,g}(1), \cdots, e_{t,g}(N-1)]^T$ with

$$e_{t,g}(n) = \bar{\mathbf{s}}'_{\mathrm{s},t,j,g}(n)/\mathbf{s}'_{\mathrm{s},t,j-1,g}(n) \tag{34}$$

Step 2. Calculate the averaged auto-correlation matrix of the CFO vector by

$$\mathbf{R}_{\mathrm{e}} = \frac{1}{T(L_{\mathrm{cp}+1})} \sum\nolimits_{t=0}^{T-1} \sum\nolimits_{g=0}^{L_{\mathrm{cp}}} \mathbf{e}_{t,g}\mathbf{e}_{t,g}^H \tag{35}$$

It is further enhanced by the FB averaging technique, obtaining $\mathbf{R}_{\mathrm{FB,e}} = \frac{1}{2}(\mathbf{R}_{\mathrm{e}} + \mathbf{J}\mathbf{R}_{\mathrm{e}}^*\mathbf{J})$.

Step 3. The remaining of the CFO estimation keeps the same to Steps 3 and 4 of the CFO estimator in Subsection III-C, but selecting one eigenvector corresponding to the largest eigenvalue only. Denote the new CFO estimate as ϕ'_j.

The rounded integer of ϕ'_j is defined as the iCFO estimate $\phi'_{\mathrm{i},j}$, while the rest is the fCFO estimate $\phi'_{\mathrm{f},j}$. The CFO-free desired channel estimate is easily obtained by $\mathbf{h}'_{\mathrm{s},j} = \mathrm{diag}\{\mathbf{e} \otimes \mathbf{1}_{N_{\mathrm{r}}\times 1}\}\bar{\mathbf{h}}'_{\mathrm{s},j}$, where $\mathbf{e} = [1, e^{-j2\pi\phi'_j/N}, \cdots, e^{-j2\pi\phi'_j(L-1)/N}]^T$. Note that the decision-directed CFO estimation can refine fCFO only. To avoid error propagation from the desired signal detection to CFO estimation, we compare the rounded integer parts of ϕ'_j and ϕ'_{j-1}. If they are equal, the CFO estimate in the j-th iteration is ϕ'_j and otherwise is ϕ'_{j-1}.

The above procedures, namely channel estimation, SI cancelation, signal detection and CFO estimation, are repeated until a satisfactory performance is obtained. Define I as the number of total iterations. Therefore, the hard decision of the desired signal has been utilized to overcome the problems resulting from the reduced training overhead due to short frames and can also enhance the system performance significantly.

V. Performance Analysis

A. CRLBs Analysis

As stated in [39], the theoretical analysis of the iterative decision-directed channel estimation is hard to make, due to its complex processing. In the following we mainly focus on the performance analysis of the initial stage of the proposed ISB receiver and derive the corresponding CRLBs for channel estimation, CFO estimation and signal detection, which serve as an analytical benchmark.

CRLB is usually obtained by taking a derivative of the received signal vector with respect to the unknown variables vector [36]. To simplify the process of derivative, we collect the received pilot and data samples in a short frame and from all the received antennas as a column vector, *i.e.*, $\mathbf{y} = [y_0^0(L-1), \cdots, y_0^0(M-1), \cdots, y_0^{N_{\mathrm{r}}-1}(L-1), \cdots, y_0^{N_{\mathrm{r}}-1}(M-1), \cdots, y_{T-1}^0(L-1), \cdots, y_{T-1}^0(M-1), \cdots, y_{T-1}^{N_{\mathrm{r}}-1}(L-1), \cdots, y_{T-1}^{N_{\mathrm{r}}-1}(M-1)]^T$, where $y_0^0(L-1)$ to $y_0^{N_{\mathrm{r}}-1}(M-1)$ are the pilot symbol samples and the rest are the data symbol samples. According to (3), $\mathbf{y}$ can be expressed as

$$\mathbf{y} = (\mathbf{I}_T \otimes ((\mathbf{I}_{N_{\mathrm{r}}} \otimes \mathbf{P})\check{\mathbf{H}}_{\mathrm{s}}\mathbf{F}_{\mathrm{all}}))\mathbf{x}_{\mathrm{s}} + \sqrt{\frac{1}{\rho}}(\mathbf{I}_T \otimes (\check{\mathbf{H}}_{\mathrm{i}}\mathbf{F}_{\mathrm{all}}))\mathbf{x}_{\mathrm{i}} + \mathbf{w} \tag{36}$$

where $\mathbf{P} = \mathrm{diag}\{[e^{j2\pi\phi(L-1)/N}, \cdots, e^{j2\pi\phi(M-1)/N}]\}$ is the CFO matrix; $\check{\mathbf{H}}_{\mathrm{s}} = [\check{\mathbf{H}}_{\mathrm{s}}^0; \check{\mathbf{H}}_{\mathrm{s}}^1; \cdots; \check{\mathbf{H}}_{\mathrm{s}}^{N_{\mathrm{r}}-1}]$ is the circulant desired channel matrix, with $\check{\mathbf{H}}_{\mathrm{s}}^{n_{\mathrm{r}}}$ of size $(M-L+1)\times M$ defined as

$$\check{\mathbf{H}}_{\mathrm{s}}^{n_{\mathrm{r}}} = \begin{bmatrix} h_{\mathrm{s}}^{n_{\mathrm{r}}}(L-1) & \cdots & h_{\mathrm{s}}^{n_{\mathrm{r}}}(0) & \cdots & \cdots & 0 \\ \vdots & \ddots & \ddots & \ddots & \ddots & \vdots \\ 0 & \cdots & \cdots & h_{\mathrm{s}}^{n_{\mathrm{r}}}(L-1) & \cdots & h_{\mathrm{s}}^{n_{\mathrm{r}}}(0) \end{bmatrix} \tag{37}$$

$\check{\mathbf{H}}_{\mathrm{i}} = [\check{\mathbf{H}}_{\mathrm{i}}^0; \check{\mathbf{H}}_{\mathrm{i}}^1; \cdots; \check{\mathbf{H}}_{\mathrm{i}}^{N_{\mathrm{r}}-1}]$, with $\check{\mathbf{H}}_{\mathrm{i}}^{n_{\mathrm{r}}}$ defined as a similar form to $\check{\mathbf{H}}_{\mathrm{s}}^{n_{\mathrm{r}}}$ but replacing $h_{\mathrm{s}}^{n_{\mathrm{r}}}(l)$ by $h_{\mathrm{i}}^{n_{\mathrm{r}}}(l)$; $\mathbf{F}_{\mathrm{all}} = [\mathbf{F}(N-L_{\mathrm{cp}}\colon N-1, 0\colon N-1); \mathbf{F}]$ with $\mathbf{F}$ denoting the IDFT matrix of size $N\times N$; $\mathbf{x}_{\mathrm{s}} = [\mathbf{x}_{\mathrm{s},0}; \mathbf{x}_{\mathrm{s,d}}]$ with $\mathbf{x}_{\mathrm{s},0}$ denoting the pilot symbol vector of the desired signal in the frequency domain and $\mathbf{x}_{\mathrm{s,d}} = [\mathbf{x}_{\mathrm{s},1}; \mathbf{x}_{\mathrm{s},2}; \cdots; \mathbf{x}_{\mathrm{s},T-1}]$ denoting the data symbol vector in the frequency domain; $\mathbf{x}_{\mathrm{i}} = [\mathbf{x}_{\mathrm{i},0}; \mathbf{x}_{\mathrm{i},1}; \cdots; \mathbf{x}_{\mathrm{i},T-1}]$ is the SI symbol vector in the frequency domain and $\mathbf{w} = [w_0^0(L-1), \cdots, w_0^0(M-1), \cdots, w_0^{N_{\mathrm{r}}-1}(L-1), \cdots, w_0^{N_{\mathrm{r}}-1}(M-1), \cdots, w_{T-1}^0(L-1), \cdots, w_{T-1}^0(M-1), \cdots, w_{T-1}^{N_{\mathrm{r}}-1}(L-1), \cdots, w_{T-1}^{N_{\mathrm{r}}-1}(M-1)]^T$ is the noise vector.

Regarding the semi-blind estimation of CFO and channel in FD systems, the unknown variables are the CFO ϕ, the desired CIR vector denoted as $\mathbf{h}_{\mathrm{s}} = [\mathbf{h}_{\mathrm{s}}(0); \cdots; \mathbf{h}_{\mathrm{s}}(L-1)]$, the SI CIR vector denoted as $\mathbf{h}_{\mathrm{i}} = [\mathbf{h}_{\mathrm{i}}(0); \cdots; \mathbf{h}_{\mathrm{i}}(L-1)]$ and the vector of the desired data symbols $\mathbf{x}_{\mathrm{s,d}}$. Note that the real and imaginary parts of the unknown complex variables should be considered separately for derivatives [36]. Then, all of the unknown variables are collected in a column vector, *i.e.*, $\boldsymbol{\Theta} = [\phi, \Re\{\mathbf{h}_{\mathrm{s}}^T\}, \Im\{\mathbf{h}_{\mathrm{s}}^T\}, \Re\{\mathbf{h}_{\mathrm{i}}^T\}, \Im\{\mathbf{h}_{\mathrm{i}}^T\}, \Re\{\mathbf{x}_{\mathrm{s,d}}^T\}, \Im\{\mathbf{x}_{\mathrm{s,d}}^T\}]^T$. Denote $\mathbf{U} = (\mathbf{I}_T \otimes ((\mathbf{I}_{N_{\mathrm{r}}} \otimes \mathbf{P})\check{\mathbf{H}}_{\mathrm{s}}\mathbf{F}_{\mathrm{all}}))\mathbf{x}_{\mathrm{s}} + \sqrt{1/\rho}(\mathbf{I}_T \otimes (\check{\mathbf{H}}_{\mathrm{i}}\mathbf{F}_{\mathrm{all}}))\mathbf{x}_{\mathrm{i}}$. According to [40], the Fisher information matrix can be given by

$$\boldsymbol{\Phi} = \frac{2}{\sigma^2}\Re[\frac{\partial \mathbf{U}^H}{\partial \boldsymbol{\theta}}\frac{\partial \mathbf{U}}{\partial \boldsymbol{\theta}^T}] \tag{38}$$

where σ^2 is the noise variance. Through some derivations, as detailed in Appendix A, we can obtain

$$\frac{\partial \mathbf{U}^H}{\partial \boldsymbol{\theta}} = [-\jmath\mathbf{G}^H; \mathbf{A}^H; -\jmath\mathbf{A}^H; \mathbf{B}^H; -\jmath\mathbf{B}^H; \mathbf{C}^H; -\jmath\mathbf{C}^H] \tag{39}$$

and

$$\frac{\partial \mathbf{U}}{\partial \boldsymbol{\theta}^T} = [\jmath\mathbf{G}, \mathbf{A}, \jmath\mathbf{A}, \mathbf{B}, \jmath\mathbf{B}, \mathbf{C}, \jmath\mathbf{C}] \tag{40}$$

where $\mathbf{G} = \frac{2\pi}{N}(\mathbf{I}_T \otimes ((\mathbf{I}_{N_{\mathrm{r}}} \otimes (\mathbf{DP}))\check{\mathbf{H}}_{\mathrm{s}}\mathbf{F}_{\mathrm{all}}))\mathbf{x}_{\mathrm{s}}$ with $\mathbf{D} = \mathrm{diag}\{[L-1, \cdots, M-1]\}$; $\mathbf{A} = [\mathbf{A}_{0,0}, \cdots, \mathbf{A}_{0,N_{\mathrm{r}}-1}, \cdots, \mathbf{A}_{L-1,0} \cdots, \mathbf{A}_{L-1,N_{\mathrm{r}}-1}]$ with

TABLE I
Number of Complex Multiplications and Additions (N: Number of subcarriers in each OFDM symbol, L_{cp}: CP length, T: Frame length, N_{r}: Number of receive antennas, L: Channel length, $M = N + L_{\text{cp}}$ and I: Number of iterations.)

Item		ISB receiver	iCFO-HD [34]+fCFO-HD [35] +ML [29]	iCFO-HD [34]+fCFO-HD [35] +Subspace [32]
Channel estimation		$(2(N-L+1)N_{\text{r}}T(L_{\text{cp}}+1)$ $+(N-L+1)^2N_{\text{r}}^2+N_{\text{r}}^2L^2N+16N^2$ $+4N(L_{\text{cp}}+1)+(22N-8)(L_{\text{cp}}+1)$ $+8N^3)(N-L+1)N_{\text{r}}+(16N_{\text{r}}^3L^2$ $+4N_{\text{r}}^2LT)(M-L+1)(I-1)$	$8N_{\text{r}}^3L^2NT+4N_{\text{r}}^2LNT$ $+8IN_{\text{r}}^2NLT(1+N_{\text{r}}N+N_{\text{r}}L)$	$2N_{\text{r}}^2M^2T+N_{\text{r}}^3M^3$ $+NN_{\text{r}}^2L^2(N_{\text{r}}M-2N)$ $+68TN+20N$
CFO estimation	iCFO	$5N^3I+4N^2L_{\text{cp}}+2N^2$ $+(2NT+1)N(L_{\text{cp}}+1)(I-1)$	$4N^3+5N^2N_{\text{r}}^2$	
	fCFO		$6N_{\text{r}}^3N\log_2N$	
SI cancelation		$2(M-L+1)MTN_{\text{r}}I$	$2(M-L+1)MTN_{\text{r}}$	
Signal detection		$I(2MN_{\text{r}}(M-L+1)(2M+T)$ $+M^3+TN\log_2N)$	$2MN_{\text{r}}(M-L+1)(2M+T)$ $+M^3+TN\log_2N$	

$\mathbf{A}_{l,n_{\text{r}}} = (\mathbf{I}_T \otimes ((\mathbf{I}_{N_{\text{r}}} \otimes \mathbf{P})\text{circshift}(\mathbf{a}_l,(M-L+1)n_{\text{r}})\mathbf{F}_{\text{all}}))\mathbf{x}_{\text{s}}$, $\mathbf{a}_l = \text{circshift}(\mathbf{a},-l,2)$, $\mathbf{a} = [\mathbf{b}_1;\mathbf{b}_2]$, $\mathbf{b}_1 = \text{toeplitz}(\mathbf{0}_{(M-L+1)\times 1},[\mathbf{0}_{1\times(L-1)},1,\mathbf{0}_{1\times(M-L)}])$ and $\mathbf{b}_2 = \mathbf{0}_{(M-L+1)(N_{\text{r}}-1)\times M}$; $\mathbf{B}$ is defined in a similar form to $\mathbf{A}$ but with $\mathbf{A}_{l,n_{\text{r}}}$ replaced by $\mathbf{B}_{l,n_{\text{r}}} = (\mathbf{I}_T \otimes (\text{circshift}(\mathbf{a}_l,(M-L+1)n_{\text{r}})\mathbf{F}_{\text{all}}))\mathbf{x}_{\text{i}}$; $\mathbf{C} = [\mathbf{C}_{0,0},\cdots,\mathbf{C}_{N-1,0},\cdots,\mathbf{C}_{0,T-2},\cdots,\mathbf{C}_{N-1,T-2}]$ with $\mathbf{C}_{n,t} = (\mathbf{I}_T \otimes ((\mathbf{I}_{N_{\text{r}}} \otimes \mathbf{P})\check{\mathbf{H}}_{\text{s}}\mathbf{F}_{\text{all}}))\text{circshift}(\mathbf{c}_n,tN)$, $\mathbf{c}_n = \text{circshift}(\mathbf{c},n)$ and $\mathbf{c} = [\mathbf{0}_{N\times 1};1;\mathbf{0}_{((T-1)N-1)\times 1}]$. Based on (38), (39) and (40), the Fisher information matrix can be easily determined and we denote it as $\mathbf{\Phi}$.

The CRLBs can be obtained using the diagonal elements of $\boldsymbol{\theta} = \mathbf{\Phi}^{-1}$ [36], [40]. The CRLBs for CFO estimation, channel estimation (including both desired and SI channels) and signal detection are respectively given by

$$\text{CRLB}_{\text{CFO}} = \boldsymbol{\theta}(0,0) \tag{41}$$

$$\text{CRLB}_{\text{channel}} = \frac{1}{2N_{\text{r}}L}\sum\nolimits_{p=1}^{4N_{\text{r}}L}\boldsymbol{\theta}(p,p) \tag{42}$$

$$\text{CRLB}_{\text{signal}} = \frac{1}{N(T-1)}\sum\nolimits_{p=1+4N_{\text{r}}L}^{2N(T-1)+4N_{\text{r}}L}\boldsymbol{\theta}(p,p) \tag{43}$$

Moreover, the output SINR can be related to the MSE of signal detection by $\text{SINR}_{\text{out}} = 1/\text{MSE}_{\text{signal}} - 1$ in [41]. Since $\text{MSE}_{\text{signal}} \geq \text{CRLB}_{\text{signal}}$, the output SINR is bounded by

$$\text{SINR}_{\text{out}} \leq \frac{1}{\text{CRLB}_{\text{signal}}} - 1 \tag{44}$$

B. Complexity Analysis

The symbolic computational complexities of the proposed ISB receiver structure and the existing methods [29], [32], [34], [35] are demonstrated in Table I, in terms of the number of complex additions and multiplications. Due to lack of integral solutions to CFO estimation and channel estimation for FD systems in the literature, iCFO-HD in [34] and fCFO-HD in [35] are exploited for iCFO and fCFO estimation, whereas the iterative ML [29] and subspace [32] methods are chosen as references for channel estimation and SI cancelation. Their complexities are compared in four aspects, namely channel estimation, CFO estimation, SI cancelation and signal detection. Regarding the proposed ISB receiver structure, the complexity of each aspect depends on the number of iterations, owing to its decision-directed estimation, while the channel estimation in [29] is iterative and the methods in [32], [34], [35] are all non-iterative. Moreover, we can see that the proposed ISB receiver structure provides an integral solution to iCFO and fCFO estimation, while the existing methods [34], [35] require two separate processes for iCFO and fCFO estimation, respectively. The signal detection algorithm in the proposed ISB receiver is shared by the reference receivers.

Based on the symbolic complexity analysis, a numerical complexity analysis is provided in Table II using the parameter settings in Section VI, where all complexities are normalized to the lowest complexity of all items, which is the complexity of the fCFO-HD estimator in [35]. The following observations can be made from Table II.

First, it can be seen that channel estimation dominates the overall complexity of all receivers. The ML [29] based channel estimation has the highest complexity. With a single iteration, the complexity of the proposed ISB receiver structure is approximately half of that of the ML method [29] and is also comparable to that of the subspace method [32]. As the number of iterations is increased to 3, the complexity of the proposed ISB receiver structure is around six-times less than that of the ML approach [29].

Second, the complexity of channel estimation in the proposed ISB receiver increases slower than that of the ML method [29] with the increase of the number of iterations, reflected by a complexity increase of 5% versus 200% as the number of iterations increases from 1 to 3. This is because regarding the proposed ISB receiver structure, the subspace based blind channel estimation at the initial stage plays a dominant role in complexity, which requires a large number of computations for auto-correlation matrix, EVD, etc, while the complexity of the ML method in [29] is high to solve the ML function and proportional to the number of iterations.

VI. Simulation Results

A. Simulation Setup

Monte Carlo simulations have been carried out to demonstrate the performance of the proposed ISB receiver structure for URLLC in a short-frame system with CFO, in comparison with the channel estimation methods based on ML [29] and subspace [32], and the CFO estimation methods of iCFO-HD [34] and fCFO-HD [35]. The signal detection algorithm in the proposed ISB receiver is shared by the reference receivers.

TABLE II
Normalized Numerical Complexity ($N = 32$, $L_{\text{cp}} = 8$, $T = 20$, $N_{\text{r}} = 4$, $L = 2$ and $M = 40$. est.: estimation, cancel.: cancelation, detect.: detection.)

Item	ISB receiver		iCFO-HD [34] +fCFO-HD [35] +ML [29]		iCFO-HD [34] +fCFO-HD [35] +Subspace [32]	
	I=1	I=3	I=1	I=3	I=1	I=3
Channel est.	161	169	369	1063	124	
iCFO est.	3	20	4			
fCFO est.			1			
SI cancel.	4	12	4			
Signal detect.	23	68	23			
Total	191	269	400	1094	155	

The dervied CRLBs in Subsection V-A are also used as benchmarks. Each frame contains $T = 20$ OFDM symbols of $N = 32$ subcarriers, except for Fig. 6 where the frame length is a variable. The CP length is $L_{\text{cp}} = 8$. Quadrature phase shift keying (QPSK) modulation is assumed. A two-ray channel model of length $L = 2$ is used. The CFO is randomly generated, whose iCFO is in the range of $[-N/2, N/2)$ and fCFO is in the range of $[-0.5, 0.5)$, except for Fig. 8. The number of receive antennas is $N_{\text{r}} = 4$, except for Fig. 9. The average SIR ρ before the digital SI cancelation is set to -20 dB. The first OFDM symbol within a frame is used as pilot for joint CFO estimation and channel ambiguities elimination. Up to 10000 channel realizations are used to meet the requirement of Monte Carlo simulations.

Other specific simulation setups in [29], [32], [34] and [35] are adopted. One pilot symbol is used for iCFO estimation in iCFO-HD [34] and two symbols each with a null-subcarrier are used for fCFO estimation in fCFO-HD [35]. As for channel estimation, 50% of a symbol is used by the subspace method [32] and 6.25% of each symbol by the ML method [29]. With a short frame length of $T = 20$, the overall training overheads of the proposed ISB receiver, the receiver with [29]+ [34]+ [35] and the receiver with [32]+ [34]+ [35] are 5%, 11% and 8%, respectively.

The MSEs of channel and fCFO estimation for the j-th iteration are respectively defined as

$$\text{MSE}_{\text{Channel},j} = \mathbb{E}\{\frac{1}{2N_{\text{r}}L}[(\mathbf{h}'_{\text{s},j} - \mathbf{h}_{\text{s}})^2 + (\mathbf{h}'_{\text{i},j} - \mathbf{h}_{\text{i}})^2]\} \quad (45)$$

$$\text{MSE}_{\text{fCFO},j} = \mathbb{E}\{(\phi'_{\text{f},j} - \phi_{\text{f}})^2\} \quad (46)$$

The output SINR is defined as the ratio of the power of the desired signal estimate to the power of the residual SI and noise after SI cancelation, *i.e.*,

$$\text{SINR}_{\text{output},j} = \frac{\sum_{t=1}^{T-1}\sum_{n=0}^{N-1}\mathbf{x}'_{\text{s},t,j}(n)}{\sum_{t=1}^{T-1}\sum_{n=0}^{N-1}(\mathbf{x}_{\text{s},t}(n) - \mathbf{x}'_{\text{s},t,j}(n))} \quad (47)$$

B. Results and Discussion

Figs. 3, 4 and 5 demonstrate respectively the FER, output SINR and MSE of channel estimation performances of the proposed ISB receiver structure in comparison to the ML [29] and subspace [32] methods with $T = 20$ symbols per frame and $N_{\text{r}} = 4$ receive antennas. The proposed ISB receiver in the presence of CFO achieves much better FER performance

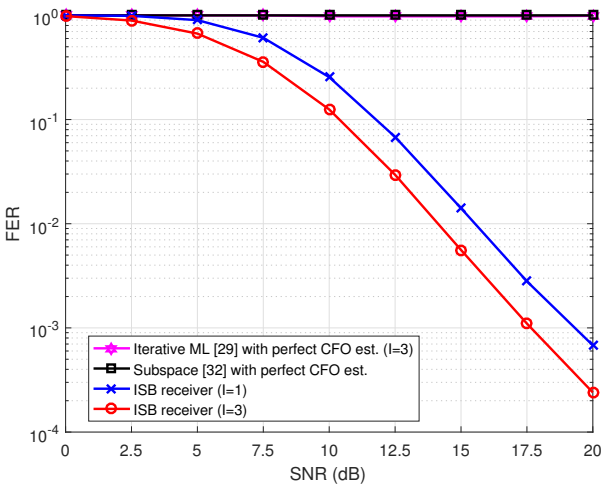

Fig. 3. FER performance of the proposed ISB receiver structure, with $T = 20$ symbols per frame and $N_{\text{r}} = 4$ receive antennas.

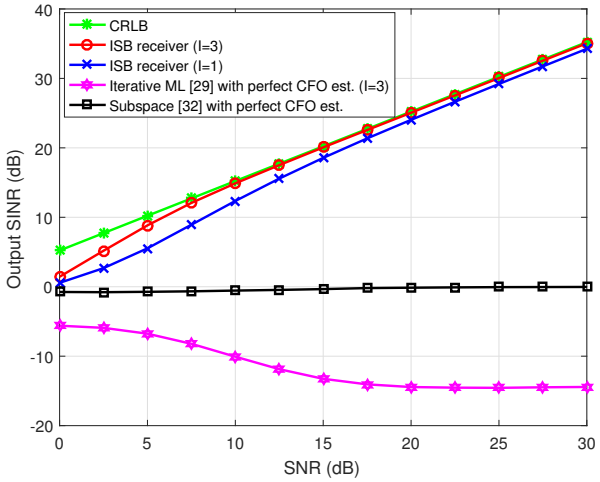

Fig. 4. Output SINR of the proposed ISB receiver structure, with $T = 20$ symbols per frame and $N_{\text{r}} = 4$ receive antennas.

than that of ML [29] and subspace [32] approaches with perfect CFO estimation, while the latter two demonstrates an error floor. This is because the ISB receiver can calculate the second-order statistics of the received signal with a short frame of data, while [29] and [32] are dependent on long data frames.

Similar trends to Fig. 3 can be observed in Fig. 4, where the output SINR by the proposed ISB receiver is much closer to the CRLB after iterations. In contrast, the output SINR by the ML approach [29] degrades slightly with the increase of signal-to-noise-ratio (SNR), because of the noise amplifications from iterations.

Fig. 5 demonstrates that at the MSE of channel estimation of 10^{-4}, the proposed ISB receiver with $I = 3$ iterations achieves an SNR gain of around 7 dB over its counterpart with one iteration. The CRLB is close to the numerical results of the ISB receiver, while ML [29] and subspace [32] demonstrate poor channel estimation accuracy across all SNRs.

Fig. 6 shows the impact of the frame length T on the

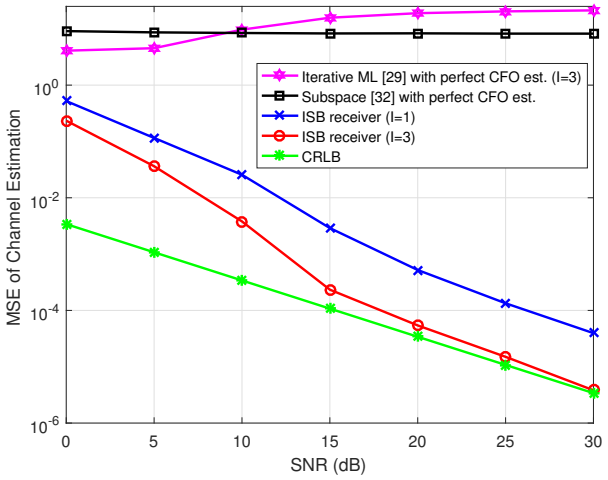

Fig. 5. MSE of channel estimation of the proposed ISB receiver structure, with $T = 20$ symbols per frame and $N_{\rm r} = 4$ receive antennas.

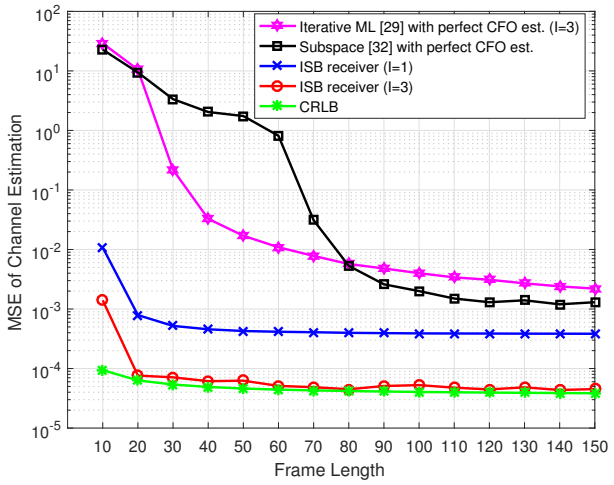

Fig. 6. Impact of the frame length on the MSE of channel estimation of the proposed ISB receiver structure, with $N_{\rm r} = 4$ receive antennas and SNR $= 20$ dB.

MSE performance of channel estimation of the proposed ISB receiver and the existing ML [29] and subspace [32] methods at SNR $= 20$ dB. It is easily observed that the proposed ISB receiver can achieve a good MSE performance while using a much shorter frame than the existing methods [29], [32]. For example, the proposed ISB receiver with three iterations can achieve MSE of 10^{-3} with 10 symbols only, while more than 100 symbols are required for the existing methods [29], [32]. This is because the number of signal samples to compute the auto-correlation matrix of the received signal is increased by the proposed ISB receiver, as discussed in Section III. Thus, it can achieve a similar performance while with a much fewer symbols. Furthermore, as the frame length increases, the training overhead of the proposed ISB receiver decreases greatly. For example, at $T = 150$, the training overhead of the proposed ISB receiver is reduced to 0.6% while that of the iterative ML method [29] is always 6.25%. Consequently, the proposed ISB receiver has advantages in both latency and spectral efficiency. Additionally, thanks to the decision-directed estimation in the proposed ISB receiver, the MSE of channel estimation is reduced by approximately ten-fold after three iterations and also approaches the derived CRLB. It is seen that the proposed ISB receiver achieves a convergence after $T = 20$. This is why the frame length is specified as 20 for the proposed ISB receiver in other figures.

To better compare the proposed ISB receiver with the existing iCFO-HD [34] and fCFO-HD [35] estimators, the CFO estimation performance of the proposed ISB receiver is studied through two aspects: a) MSE of fCFO estimation and b) probability of correct iCFO estimation. Fig. 7 exhibits the MSE of fCFO estimation of the proposed ISB receiver, in comparison to the existing method [35]. We can see that the proposed ISB receiver with a single iteration is slightly better than fCFO-HD [35]. However, after three iterations, the proposed ISB receiver demonstrates a much better performance than the existing fCFO-HD [35] especially at high SNRs. For instance, at $\text{MSE}_{\text{fCFO}} = 10^{-5}$, the proposed ISB receiver has

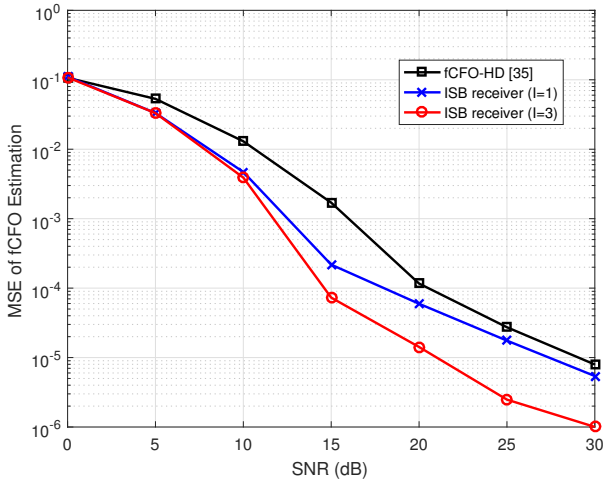

Fig. 7. MSE of fCFO estimation of the proposed ISB receiver structure, with $T = 20$ symbols per frame and $N_{\rm r} = 4$ receive antennas.

an SNR gain of around 9 dB over the fCFO-HD [35] estimator.

The probability of correct iCFO estimation of the proposed ISB receiver and the existing iCFO-HD estimator [34] is studied in Fig. 8, with two iCFO estimation ranges $[-N/2, N/2)$ and $[-N/8, N/8)$. It is noteworthy that the existing iCFO estimator [34] allows a certain iCFO estimation range only which is determined by its algorithm parameter. Also, the estimation range should be known in advance for the following iCFO search. In contrast, the proposed ISB receiver not only enables full-range iCFO estimation but also provides a closed-form solution without an advanced acquisition of iCFO estimation range. It is easily observed from Fig. 8 that the existing iCFO estimator [34] is susceptible to iCFO estimation range, while the proposed ISB receiver is almost independent of that. Specifically, the probability of correct iCFO estimation decreases greatly as the estimation range widens especially at low SNRs for the iCFO-HD estimator [34]. As mentioned

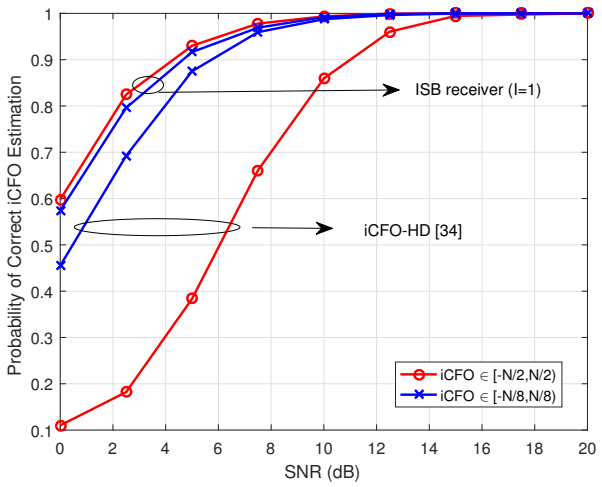

Fig. 8. Impact of the iCFO estimation range on the probability of correct iCFO estimation of the proposed ISB receiver structure, with $T = 20$ symbols per frame and $N_{\mathrm{r}} = 4$ receive antennas.

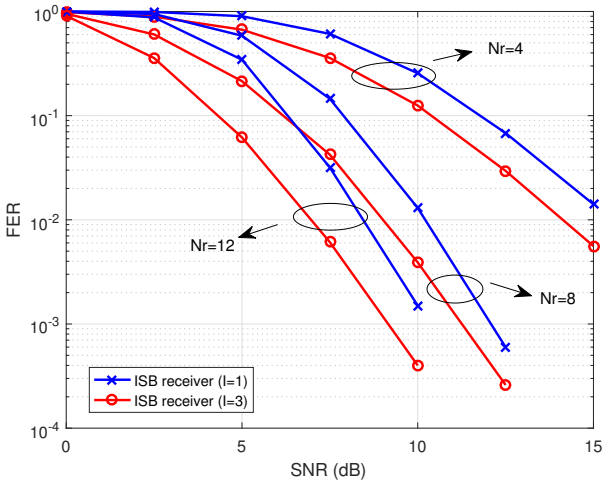

Fig. 9. Impact of the number of receive antennas N_{r} on the FER performance of the proposed ISB receiver structure, with $T = 20$ symbols per frame.

in Section IV, decision-directed CFO estimation refines fCFO only, the probability of iCFO estimation tends not to vary with the number of iterations. Thus, we only illustrate the proposed ISB receiver with a single iteration in Fig. 8.

Fig. 9 shows the impact of receive antennas on FER performance of the proposed ISB receiver, with $N_{\mathrm{r}} = 4$, $N_{\mathrm{r}} = 8$ and $N_{\mathrm{r}} = 12$, respectively. It can be concluded that the reliability of the proposed ISB receiver can be enhanced significantly by utilizing more receive antennas at the receiver. Thus, space diversity is an effective technique for URLLC, as suggested in [1].

Fig. 10 demonstrates the MSE of channel estimation against the number of iterations of the proposed ISB receiver at SNR=10 dB and SNR=15 dB, respectively. We can observe that the proposed receiver converges fast within 3 iterations. At SNR=15 dB, the initial MSE performance is improved around 10-fold after three iterations.

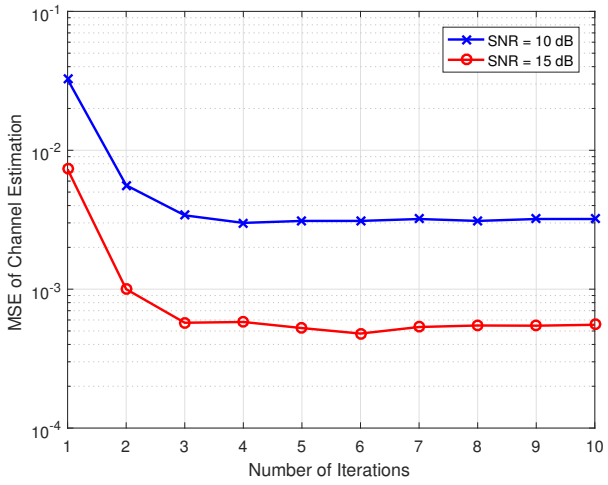

Fig. 10. Impact of the number of iterations on the MSE of channel estimation of the proposed ISB receiver structure at SNR=10 dB and SNR=15 dB, with $T = 20$ symbols per frame and $N_{\mathrm{r}} = 4$ receive antennas.

VII. Conclusion

An ISB receiver structure with CFO and channel estimation and signal detection has been proposed for URLLC in short-frame FD CP-OFDM systems. Extensive performance metrics have been assessed, including FER, MSE of channel estimation and fCFO estimation, probability of correct iCFO estimation and output SINR. Compared to the approaches in [29], [32], [34] and [35], the proposed ISB receiver achieves much better performance in short-frame case at almost a halved training overhead, requiring a single pilot only. The CRLBs derived are close to the numerical results. The FER performance can be enhanced greatly by utilizing more receive antennas. The proposed receiver can converge within 3 iterations, and is also more computationally efficient than the iterative ML approach [29].

Appendix A
Derivation of (39) and (40)

It can be shown that $\frac{\partial \mathbf{U}^H}{\partial \boldsymbol{\theta}}$ and $\frac{\partial \mathbf{U}}{\partial \boldsymbol{\theta}^T}$ can be formulated as

$$\begin{aligned}\frac{\partial \mathbf{U}^H}{\partial \boldsymbol{\theta}} =&[\frac{\partial \mathbf{U}^H}{\partial \phi}; \frac{\partial \mathbf{U}^H}{\partial \Re\{\mathbf{h}_{\mathrm{s}}\}}; \frac{\partial \mathbf{U}^H}{\partial \Im\{\mathbf{h}_{\mathrm{s}}\}};\\ &\frac{\partial \mathbf{U}^H}{\partial \Re\{\mathbf{h}_{\mathrm{i}}\}}; \frac{\partial \mathbf{U}^H}{\partial \Im\{\mathbf{h}_{\mathrm{i}}\}}; \frac{\partial \mathbf{U}^H}{\partial \Re\{\mathbf{x}_{\mathrm{s,d}}\}}; \frac{\partial \mathbf{U}^H}{\partial \Im\{\mathbf{x}_{\mathrm{s,d}}\}}]\end{aligned} \tag{48}$$

and

$$\begin{aligned}\frac{\partial \mathbf{U}}{\partial \boldsymbol{\theta}^T} =&[\frac{\partial \mathbf{U}}{\partial \phi}, \frac{\partial \mathbf{U}}{\partial \Re\{\mathbf{h}_{\mathrm{s}}^T\}}, \frac{\partial \mathbf{U}}{\partial \Im\{\mathbf{h}_{\mathrm{s}}^T\}},\\ &\frac{\partial \mathbf{U}}{\partial \Re\{\mathbf{h}_{\mathrm{i}}^T\}}, \frac{\partial \mathbf{U}}{\partial \Im\{\mathbf{h}_{\mathrm{i}}^T\}}, \frac{\partial \mathbf{U}}{\partial \Re\{\mathbf{x}_{\mathrm{s,d}}^T\}}, \frac{\partial \mathbf{U}}{\partial \Im\{\mathbf{x}_{\mathrm{s,d}}^T\}}]\end{aligned} \tag{49}$$

According to the matrix derivatives rules, we can obtain

$$\frac{\partial \mathbf{U}}{\partial \phi} = \jmath \mathbf{G}, \quad \frac{\partial \mathbf{U}^H}{\partial \phi} = -\jmath \mathbf{G}^H \tag{50}$$

$$\frac{\partial \mathbf{U}}{\partial \Re\{\mathbf{h}_{\mathrm{s}}^T\}} = \mathbf{A}, \quad \frac{\partial \mathbf{U}^H}{\partial \Re\{\mathbf{h}_{\mathrm{s}}\}} = \mathbf{A}^H \tag{51}$$

$$\frac{\partial \mathbf{U}}{\partial \Im\{\mathbf{h}_{\mathrm{s}}^T\}} = \jmath\mathbf{A}, \quad \frac{\partial \mathbf{U}^H}{\partial \Im\{\mathbf{h}_{\mathrm{s}}\}} = -\jmath\mathbf{A}^H \tag{52}$$

$$\frac{\partial \mathbf{U}}{\partial \Re\{\mathbf{h}_{\mathrm{i}}^T\}} = \mathbf{B}, \quad \frac{\partial \mathbf{U}^H}{\partial \Re\{\mathbf{h}_{\mathrm{i}}\}} = \mathbf{B}^H \tag{53}$$

$$\frac{\partial \mathbf{U}}{\partial \Im\{\mathbf{h}_{\mathrm{i}}^T\}} = \jmath\mathbf{B}, \quad \frac{\partial \mathbf{U}^H}{\partial \Im\{\mathbf{h}_{\mathrm{i}}\}} = -\jmath\mathbf{B}^H \tag{54}$$

$$\frac{\partial \mathbf{U}}{\partial \Re\{\mathbf{x}_{\mathrm{s}}^T\}} = \mathbf{C}, \quad \frac{\partial \mathbf{U}^H}{\partial \Re\{\mathbf{x}_{\mathrm{s}}\}} = \mathbf{C}^H \tag{55}$$

and

$$\frac{\partial \mathbf{U}}{\partial \Im\{\mathbf{x}_{\mathrm{s}}^T\}} = \jmath\mathbf{C}, \quad \frac{\partial \mathbf{U}^H}{\partial \Im\{\mathbf{x}_{\mathrm{s}}\}} = -\jmath\mathbf{C}^H \tag{56}$$

where $\mathbf{G} = \frac{2\pi}{N}(\mathbf{I}_T \otimes ((\mathbf{I}_{N_{\mathrm{r}}} \otimes (\mathbf{DP}))\check{\mathbf{H}}_{\mathrm{s}}\mathbf{F}_{\mathrm{all}}))\mathbf{x}_{\mathrm{s}}$ with $\mathbf{D} = \mathrm{diag}\{[L-1, \cdots, M-1]\}$; $\mathbf{A} = [\mathbf{A}_{0,0}, \cdots, \mathbf{A}_{0,N_{\mathrm{r}}-1}, \cdots, \mathbf{A}_{L-1,0} \cdots, \mathbf{A}_{L-1,N_{\mathrm{r}}-1}]$ with $\mathbf{A}_{l,n_{\mathrm{r}}} = (\mathbf{I}_T \otimes ((\mathbf{I}_{N_{\mathrm{r}}} \otimes \mathbf{P})\mathrm{circshift}(\mathbf{a}_l, (M-L+1)n_{\mathrm{r}})\mathbf{F}_{\mathrm{all}}))\mathbf{x}_{\mathrm{s}}$, $\mathbf{a}_l = \mathrm{circshift}(\mathbf{a}, -l, 2)$, $\mathbf{a} = [\mathbf{b}_1; \mathbf{b}_2]$, $\mathbf{b}_1 = \mathrm{toeplitz}(\mathbf{0}_{(M-L+1)\times 1}, [\mathbf{0}_{1\times(L-1)}, 1, \mathbf{0}_{1\times(M-L)}])$ and $\mathbf{b}_2 = \mathbf{0}_{(M-L+1)(N_{\mathrm{r}}-1)\times M}$; $\mathbf{B}$ is defined in a similar form to $\mathbf{A}$ but with $\mathbf{A}_{l,n_{\mathrm{r}}}$ replaced by $\mathbf{B}_{l,n_{\mathrm{r}}} = (\mathbf{I}_T \otimes (\mathrm{circshift}(\mathbf{a}_l, (M-L+1)n_{\mathrm{r}})\mathbf{F}_{\mathrm{all}}))\mathbf{x}_{\mathrm{i}}$; $\mathbf{C} = [\mathbf{C}_{0,0}, \cdots, \mathbf{C}_{N-1,0}, \cdots, \mathbf{C}_{0,T-2}, \cdots, \mathbf{C}_{N-1,T-2}]$ with $\mathbf{C}_{n,t} = (\mathbf{I}_T \otimes ((\mathbf{I}_{N_{\mathrm{r}}} \otimes \mathbf{P})\check{\mathbf{H}}_{\mathrm{s}}\mathbf{F}_{\mathrm{all}}))\mathrm{circshift}(\mathbf{c}_n, tN)$, $\mathbf{c}_n = \mathrm{circshift}(\mathbf{c}, n)$ and $\mathbf{c} = [\mathbf{0}_{N\times 1}; 1; \mathbf{0}_{((T-1)N-1)\times 1}]$.

REFERENCES

[1] G. Pocovi, H. Shariatmadari, G. Berardinelli, K. Pedersen, J. Steiner, and Z. Li, "Achieving ultra-reliable low-latency communications: Challenges and envisioned system enhancements," *IEEE Network*, vol. 32, no. 2, pp. 8–15, Mar. 2018.

[2] I. Parvez, A. Rahmati, I. Guvenc, A. I. Sarwat, and H. Dai, "A survey on low latency towards 5G: RAN, core network and caching solutions," *IEEE Commun. Surveys and Tutorials*, vol. 20, no. 4, pp. 3098–3130, Fourthquarter 2018.

[3] G. J. Sutton, J. Zeng, R. P. Liu, W. Ni, D. N. Nguyen, B. A. Jayawickrama, X. Huang, M. Abolhasan, and Z. Zhang, "Enabling ultra-reliable and low-latency communications through unlicensed spectrum," *IEEE Network*, vol. 32, no. 2, pp. 70–77, Mar. 2018.

[4] J. Sachs, G. Wikstrom, T. Dudda, R. Baldemair, and K. Kittichokechai, "5G radio network design for ultra-reliable low-latency communication," *IEEE Network*, vol. 32, no. 2, pp. 24–31, Mar. 2018.

[5] H. Chen, R. Abbas, P. Cheng, M. Shirvanimoghaddam, W. Hardjawana, W. Bao, Y. Li, and B. Vucetic, "Ultra-reliable low latency cellular networks: Use cases, challenges and approaches," *arXiv preprint arXiv:1709.00560*, 2017.

[6] M. Sybis, K. Wesolowski, K. Jayasinghe, V. Venkatasubramanian, and V. Vukadinovic, "Channel coding for ultra-reliable low-latency communication in 5G systems," in *Proc. IEEE VTC-Fall 2016*, Montreal, QC, Canada, Sep. 2016, pp. 1–5.

[7] G. Durisi, T. Koch, and P. Popovski, "Toward massive, ultrareliable, and low-latency wireless communication with short packets," *Proceedings of the IEEE*, vol. 104, no. 9, pp. 1711–1726, Sep. 2016.

[8] B. Lee, S. Park, D. J. Love, H. Ji, and B. Shim, "Packet structure and receiver design for low latency wireless communications with ultra-short packets," *IEEE Trans. Commun.*, vol. 66, no. 2, pp. 796–807, Feb. 2018.

[9] O. L. A. Lopez, E. M. G. Fernndez, R. D. Souza, and H. Alves, "Ultra-reliable cooperative short-packet communications with wireless energy transfer," *IEEE Sensors Journal*, vol. 18, no. 5, pp. 2161–2177, Mar. 2018.

[10] M. Matth, L. L. Mendes, N. Michailow, D. Zhang, and G. Fettweis, "Widely linear estimation for space-time-coded GFDM in low-latency applications," *IEEE Trans. Commun.*, vol. 63, no. 11, pp. 4501–4509, Nov. 2015.

[11] F. Schaich, T. Wild, and Y. Chen, "Waveform contenders for 5G - suitability for short packet and low latency transmissions," in *Proc. IEEE VTC Spring 2014*, Seoul, South Korea, May 2014, pp. 1–5.

[12] X. Sun, S. Yan, N. Yang, Z. Ding, C. Shen, and Z. Zhong, "Short-packet downlink transmission with non-orthogonal multiple access," *IEEE Trans. Wireless Commun.*, pp. 1–1, 2018.

[13] Y. Yu, H. Chen, Y. Li, Z. Ding, and B. Vucetic, "On the performance of non-orthogonal multiple access in short-packet communications," *IEEE Commun. Letters*, vol. 22, no. 3, pp. 590–593, Mar. 2018.

[14] A. Azari, P. Popovski, G. Miao, and C. Stefanovic, "Grant-free radio access for short-packet communications over 5G networks," in *Proc. IEEE GLOBECOM 2017*, Singapore, Dec. 2017, pp. 1–7.

[15] Y. Gu, H. Chen, Y. Li, and B. Vucetic, "Ultra-reliable short-packet communications: Half-duplex or full-duplex relaying?" *IEEE Wireless Commun. Letters*, pp. 1–1, 2017.

[16] F. E. Airod, H. Chafnaji, and H. Yanikomeroglu, "Performance analysis of low latency multiple full-duplex selective decode and forward relays," *arXiv preprint arXiv:1802.04076*, 2018.

[17] T. A. Khan, R. W. Heath, and P. Popovski, "Wirelessly powered communication networks with short packets," *IEEE Trans. Commun.*, vol. 65, no. 12, pp. 5529–5543, Dec. 2017.

[18] S. S. Ullah, G. Liva, and S. C. Liew, "Short packet physical-layer network coding with mismatched channel state information," in *Proc. IEEE WCNC 2018*, Barcelona, Spain, Apr. 2018, pp. 1–5.

[19] M. Mousaei and B. Smida, "Optimizing pilot overhead for ultra-reliable short-packet transmission," in *Proc. IEEE ICC 2017*, Paris, France, May 2017, pp. 1–5.

[20] M. G. Sarret, G. Berardinelli, N. H. Mahmood, and P. Mogensen, "Can full duplex boost throughput and delay of 5G ultra-dense small cell networks?" in *Proc. IEEE VTC Spring 2016*, Nanjing, China, May 2016, pp. 1–5.

[21] Z. Wei, X. Zhu, S. Sun, Y. Huang, L. Dong, and Y. Jiang, "Full-duplex versus half-duplex amplify-and-forward relaying: Which is more energy efficient in 60-ghz dual-hop indoor wireless systems?" *IEEE J. Sel. Areas Commun.*, vol. 33, no. 12, pp. 2936–2947, Dec. 2015.

[22] M. Duarte, C. Dick, and A. Sabharwal, "Experiment-driven characterization of full-duplex wireless systems," *IEEE Trans. Wireless Commun.*, vol. 11, no. 12, pp. 4296–4307, Dec. 2012.

[23] E. Everett, A. Sahai, and A. Sabharwal, "Passive self-interference suppression for full-duplex infrastructure nodes," *IEEE Trans. Wireless Commun.*, vol. 13, no. 2, pp. 680–694, Feb. 2014.

[24] J. H. Lee, "Self-interference cancelation using phase rotation in full-duplex wireless," *IEEE Trans. Veh. Technol.*, vol. 62, no. 9, pp. 4421–4429, Nov. 2013.

[25] A. Koohian, H. Mehrpouyan, A. A. Nasir, S. Durrani, and S. D. Blostein, "Residual self-interference cancellation and data detection in full-duplex communication systems," in *Proc. IEEE ICC 2017*, Paris, France, May 2017, pp. 1–6.

[26] S. Shaboyan, E. Ahmed, A. S. Behbahani, W. Younis, and A. M. Eltawil, "Frequency and timing synchronization for in-band full-duplex OFDM system," in *Porc. IEEE GLOBECOM 2017*, Singapore, Dec. 2017, pp. 1–7.

[27] H. Lee, J. Choi, D. Kim, and D. Hong, "Impact of time and frequency misalignments in OFDM based in-band full-duplex systems," in *Proc. IEEE WCNC 2017*, San Francisco, CA, USA, Mar. 2017, pp. 1–6.

[28] S. Li and R. D. Murch, "An investigation into baseband techniques for single-channel full-duplex wireless communication systems," *IEEE Trans. Wireless Commun.*, vol. 13, no. 9, pp. 4794–4806, Sep. 2014.

[29] A. Masmoudi and T. Le-Ngoc, "A maximum-likelihood channel estimator for self-interference cancelation in full-duplex systems," *IEEE Trans. Veh. Technol.*, vol. 65, no. 7, pp. 5122–5132, Jul. 2016.

[30] F. Shu, J. Wang, J. Li, R. Chen, and W. Chen, "Pilot optimization, channel estimation, and optimal detection for full-duplex OFDM systems with IQ imbalances," *IEEE Trans. Veh. Technol.*, vol. 66, no. 8, pp. 6993–7009, Aug. 2017.

[31] D. Korpi, L. Anttila, V. Syrjl, and M. Valkama, "Widely linear digital self-interference cancellation in direct-conversion full-duplex transceiver," *IEEE J. Sel. Areas Commun.*, vol. 32, no. 9, pp. 1674–1687, Sep. 2014.

[32] A. Masmoudi and T. Le-Ngoc, "Channel estimation and self-interference cancelation in full-duplex communication systems," *IEEE Trans. Veh. Technol.*, vol. 66, no. 1, pp. 321–334, Jan. 2017.

[33] Y. Zeng, A. R. Leyman, and T. S. Ng, "Joint semiblind frequency offset and channel estimation for multiuser MIMO-OFDM uplink," *IEEE Trans. Commun.*, vol. 55, no. 12, pp. 2270–2278, Dec. 2007.

[34] Y. Jiang, H. Minn, X. Gao, X. You, and Y. Li, "Frequency offset estimation and training sequence design for MIMO OFDM," *IEEE Trans. Wireless Commun.*, vol. 7, no. 4, pp. 1244–1254, Apr. 2008.

[35] W. Zhang, Q. Yin, and W. Wang, "Blind closed-form carrier frequency offset estimation for OFDM with multi-antenna receiver," *IEEE Trans. Veh. Technol.*, vol. 64, no. 8, pp. 3850–3856, Aug. 2015.
[36] F. Gao, Y. Zeng, A. Nallanathan, and T. S. Ng, "Robust subspace blind channel estimation for cyclic prefixed MIMO ODFM systems: algorithm, identifiability and performance analysis," *IEEE J. Sel. Areas Commun.*, vol. 26, no. 2, pp. 378–388, Feb. 2008.
[37] C. Shin, R. W. Heath, and E. J. Powers, "Blind channel estimation for MIMO-OFDM systems," *IEEE Trans. Veh. Technol.*, vol. 56, no. 2, pp. 670–685, Mar. 2007.
[38] Y. Liu, Z. Tan, H. Hu, L. J. Cimini, and G. Y. Li, "Channel estimation for OFDM," *IEEE Commun. Surveys and Tutorials*, vol. 16, no. 4, pp. 1891–1908, Oct. 2014.
[39] C. Wei and D. W. Lin, "A decision-directed channel estimator for OFDM-based bursty vehicular communication," *IEEE Trans. Veh. Technol.*, vol. 66, no. 6, pp. 4938–4953, Jun. 2017.
[40] J. Chen, Y. Wu, S. Ma, and T. Ng, "Joint CFO and channel estimation for multiuser MIMO-OFDM systems with optimal training sequences," *IEEE Trans. Signal Process.*, vol. 56, no. 8, pp. 4008–4019, Aug. 2008.
[41] J. M. Cioffi, G. P. Dudevoir, M. V. Eyuboglu, and G. D. Forney, "MMSE decision-feedback equalizers and coding. I. Equalization results," *IEEE Trans. Commun.*, vol. 43, no. 10, pp. 2582–2594, Oct. 1995.

Yujie Liu (S'17) received the B.Eng. degree in electrical engineering and electronics from the University of Liverpool, Liverpool, U.K., China, in 2014, the M.Sc. degree in Communications and Signal Processing from Imperial College London, London, U.K., in 2015. She is currently pursuing the Ph.D. degree with the Department of Electrical Engineering and Electronics, University of Liverpool, and the Department of Electrical and Electronic Engineering, Xi'an Jiaotong-Liverpool University. Her research interests include frequency synchronization, blind channel estimation, full-duplex and GFDM.

Xu Zhu (S'02-M'03-SM'12) received the B.Eng. degree (with the first-class Hons.) in electronics and information engineering from Huazhong University of Science and Technology, Wuhan, China, in 1999, and the Ph.D. degree in electrical and electronic engineering from the Hong Kong University of Science and Technology, Hong Kong, in 2003. She joined the Department of Electrical Engineering and Electronics, the University of Liverpool, Liverpool, U.K. in 2003 as an academic member, where she is currently a Reader. She has over 160 peer-reviewed publications on communications and signal processing. Her research interests include MIMO, channel estimation and equalization, resource allocation, cooperative communications, green communications, etc. She has acted as a chair for various international conferences, such as Symposium Co-Chair of IEEE ICC 2016 and 2019, Vice-Chair of the 2006 and 2008 ICARN International Workshops, Program Chair of ICSAI 2012, and Publicity Chair of IEEE IUCC-2016. She has served as an Editor for the IEEE TRANSACTIONS ON WIRELESS COMMUNICATIONS and a Guest Editor for several international journals such as Electronics.

Eng Gee Lim (SM'12) received the B.Eng (Hons) and Ph.D degrees in electrical and electronic engineering from the University of Northumbria, U.K.. He was with Andrew Ltd. from 2002 to 2007, a leading communications systems company. Since 2007, he has been with Xi'an Jiaotong-Liverpool University, where he is currently the University Dean of Research and Graduate studies, the Director of AI University Research Centre, and also a Professor with the Department of Electrical and Electronic Engineering. He has published over 100 refereed international journals and conference papers. His research interests are Artificial Intelligence, robotics, AI+ Health care, international Standard (ISO/ IEC) in Robotics, antennas, RF/microwave engineering, EM measurements/simulations, energy harvesting, power/energy transfer, smart-grid communication; wireless communication networks for smart and green cities. He is a charter engineer and Fellow of IET and IEAust. In addition, he is also a senior fellow of HEA.

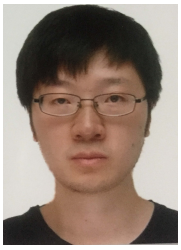

Yufei Jiang (S'12-M'14) received the Ph.D. degree in electrical engineering and electronics from the University of Liverpool, Liverpool, U.K., in 2014. From 2014 to 2015, he was a Post-Doc Researcher with the Department of Electrical Engineering and Electronic, University of Liverpool. From 2015 to 2017, he was a Research Associate with the Institutes for Digital Communications, University of Edinburgh, Edinburgh, U.K.. He is currently an Assistant Professor with the Harbin Institute of Technology, Shenzhen, China. His research interests include LiFi, synchronization, full-duplex, blind source separation, etc.

Yi Huang (S'91-M'96-SM'06) received B.Sc in Physics (Wuhan University, China) in 1984, M.Sc (Eng) in Microwave Engineering (NRIET, Nanjing, China) in 1987, and DPhil in Communications from the University of Oxford, UK in 1994.

His experience includes three years spent with NRIET as a Radar Engineer and various periods with the Universities of Birmingham, Oxford, and Essex at the U.K., as a Member of Research Staff. He was a Research Fellow of British Telecom Labs in 1994, and then joined the Department of Electrical Engineering and Electronics, University of Liverpool, U.K., as a Faculty Member, in 1995, where he is currently a Full Professor in wireless engineering, the Head of the High Frequency Engineering Group, and the Deputy Head of the Department. Since 1987, he has been conducting research in the areas of wireless communications, applied electromagnetics, radar and antennas. He is a Fellow of the IET and a Senior Fellow of the HEA. He has acted as a consultant to various companies. He has published over 350 refereed papers in leading international journals and conference proceedings. He has authored *Antennas: from Theory to Practice (John Wiley, 2008)* and *Reverberation Chambers: Theory and Applications to EMC and Antenna Measurements (John Wiley, 2016)*. He has received many research grants from research councils, government agencies, charity, EU and industry. He has served for a number of national and international technical committees. He has been a Keynote/Invited Speaker and Organiser of many conferences and workshops (e.g. WiCom 2006, 2010, and the IEEE iWAT2010, LAPC2012 and EuCAP2018). He has been an Editor, Associate Editor, or Guest Editor of five international journals. He is currently the Editor-in-Chief of *Wireless Engineering and Technology*, and an Associate Editor of IEEE Antennas and Wireless Propagation Letters, U.K., and *European Association of Antenna and Propagation*, Ireland.